Quaternary Science Reviews 200 (2018) 287–312

Contents lists available at ScienceDirect

Quaternary Science Reviews

journal homepage: www.elsevier.com/locate/quascirev

Asynchronous glacier dynamics during the Antarctic Cold Reversal in central Patagonia

B.J. Davies [a, *], V.R. Thorndycraft [a], D. Fabel [b], J.R.V. Martin [a]

[a] Centre for Quaternary Research, Department of Geography, Royal Holloway University of London, Egham, Surrey, TW20 0EX, UK
[b] SUERC AMS Laboratory, Scottish Universities Environmental Research Centre (SUERC), University of Glasgow, Rankine Avenue, East Kilbride, G75 0QF, UK

ARTICLE INFO

Article history:
Received 19 July 2018
Received in revised form
17 September 2018
Accepted 18 September 2018

ABSTRACT

We present 14 new ^{10}Be cosmogenic nuclide exposure ages quantifying asynchronous readvances during the Antarctic Cold Reversal from glaciers in the Baker Valley region of central Patagonia. We constrain glacier and ice-dammed palaeolake dynamics using a landsystems approach, concentrating on outlet glaciers from the eastern Northern Patagonian Icefield (NPI) and Monte San Lorenzo (MSL). Soler Glacier (NPI) produced lateral moraines above Lago Bertrand from 15.1 ± 0.7 to 14.0 ± 0.6 ka, when it dammed the drainage of Lago General Carrera/Buenos Aires through Río Baker at a bedrock pinning point. At this time, Soler Glacier terminated into the 400 m "Deseado" level of the ice-dammed palaeolake. Later, Calluqueo Glacier (MSL) deposited subaerial and subaqueous moraines in the Salto Valley near Cochrane at 13.0 ± 0.6 ka. These moraines were deposited in an ice-dammed palaeolake unified through the Baker Valley (Lago Chalenko; 350 m asl). The Salto Valley glaciolacustrine landsystem includes subaqueous morainal banks, ice-scoured bedrock, glacial diamicton plastered onto valley sides, perched delta terraces, kame terraces, ice-contact fans, palaeoshorelines and subaerial push and lateral moraines. Boulders from the subaqueous Salto Moraine became exposed at 12.1 ± 0.6 years, indicating palaeolake drainage. These data show an asynchronous advance of outlet glaciers from the Northern Patagonian Icefield and Monte San Lorenzo during the Antarctic Cold Reversal. These advances occurred during a period of regional climatic cooling, but differential moraine extent and timing of advance was controlled by topography and calving processes.

1. Introduction

1.1. Late Quaternary palaeoclimate and the Patagonian Ice Sheet

During the Last Glacial Termination in the Southern Hemisphere, a phase of warming atmospheric and ocean temperatures from ~18.0 ka was interrupted by cooling during the Antarctic Cold Reversal (ACR; 14.7 to 13.0 ka) (Jouzel et al., 2001; Morgan, 2009; Putnam et al., 2010; Pedro et al., 2016). The ACR dominates Southern Hemisphere palaeoclimate records up to at least 40°S (Pedro et al., 2016), therefore potentially affecting glaciers of the Northern Patagonian Icefield and Monte San Lorenzo ice cap (NPI and MSL, respectively; Fig. 1) in the Patagonian Andes of South America. Glacier readvances during the ACR have been documented in the tropical Andes (10–20°S) (Jomelli et al., 2014, 2017), for Colonia Glacier of the NPI (Nimick et al., 2016), for Tranquilo Glacier of MSL (Sagredo et al., 2018), in Cordillera Darwin (54°S) (Menounos et al., 2013), and in Torres del Paine (51°S) (Fogwill and Kubik, 2005; García et al., 2012). However, some have argued that a significant readvance also occurred during the Northern Hemisphere Younger Dryas (Ackert et al., 2008; Glasser et al., 2012, 2016; Rasmussen et al., 2014; Nimick et al., 2016). Palaeoclimatic controls on glaciers and the role of the bi-hemisphere seesaw (Pedro et al., 2018) in modulating climate in central Patagonia therefore remain poorly resolved.

Topographic controls and glaciolacustrine dynamics also have the potential to influence the timing of moraine formation (Barr and Lovell, 2014), which may account for the range of published ages from ~15.0 to ~10.0 ka for moraines at broadly coincident ice margin positions in this region (e.g. Glasser et al., 2012; Nimick et al., 2016). In order to use the geomorphic record of glacier advances as proxy data for reconstructing the structure of these past climatic changes, detailed landform mapping and geochronological data are required from a larger sample of moraines. Furthermore,

* Corresponding author.
E-mail address: bethan.davies@rhul.ac.uk (B.J. Davies).

https://doi.org/10.1016/j.quascirev.2018.09.025

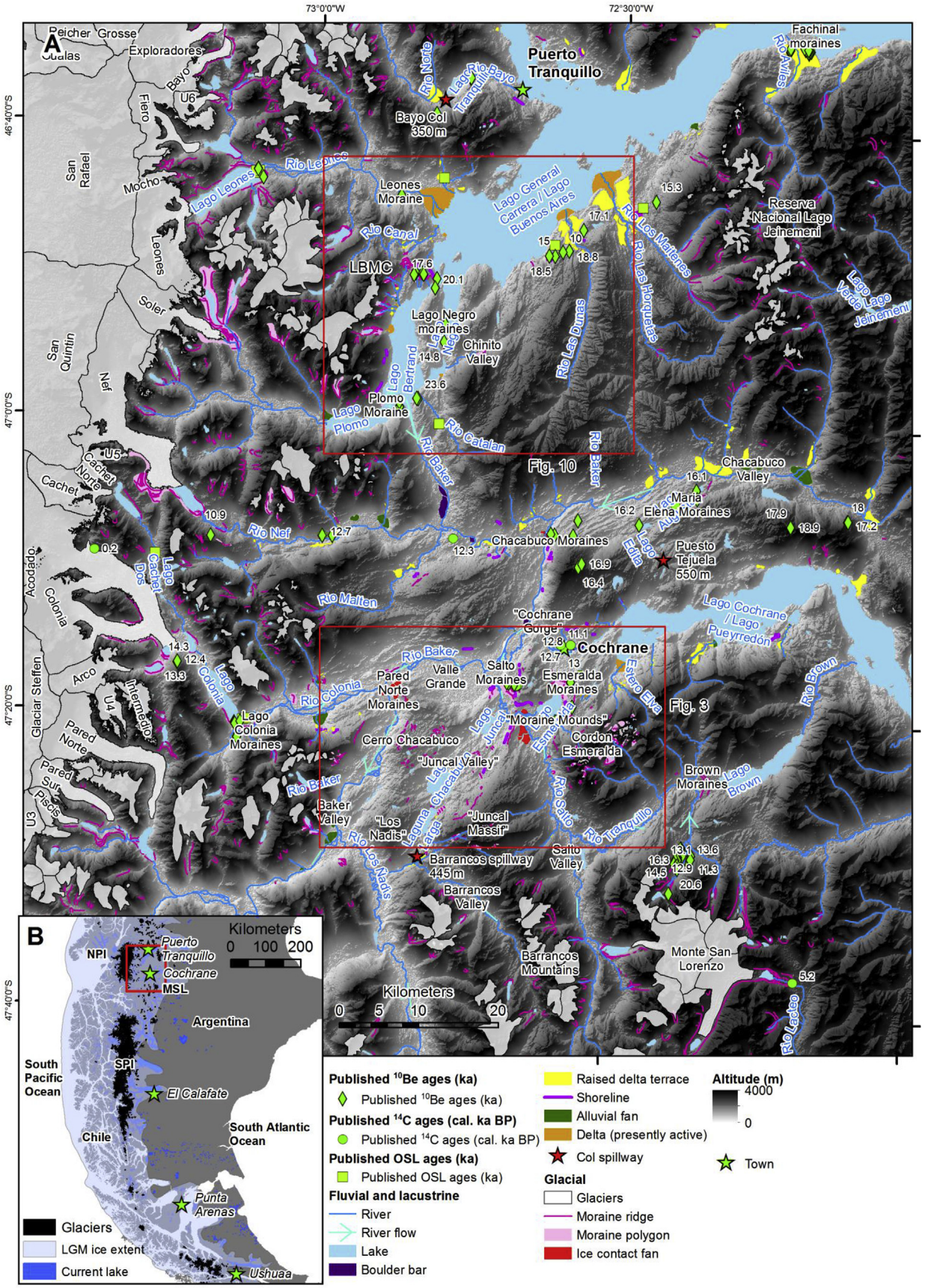

Fig. 1. A. Regional overview of study area, showing rivers, lakes, glaciers and key geomorphology. Moraines and sandar are modified from Glasser and Jansson (2008). Delta terraces modified from various authors (Bell, 2008; Bell, 2009; Bourgois et al., 2016; Glasser et al., 2016; Bendle et al., 2017b; Thorndycraft et al., 2018). Boulder bars from Thorndycraft et al.

detailed mapping of morphostratigraphic relationships between glacial and glaciolacustrine landforms is required to elucidate glacier-glaciolacustrine dynamics.

1.2. Aims and objectives

We aim to test the synchronicity of glacier behaviour in the Baker Valley region of the central Patagonian Andes (Fig. 1) during the Last Glacial Termination and elucidate palaeoclimatic and topographic controls on moraine formation through new geomorphic mapping and cosmogenic exposure-age dating from previously undated ice margins of both NPI and MSL outlet glaciers. These moraines are all well inside the Last Glacial Maximum (LGM) limits but beyond moraines dated to ca. 11 ka (Fig. 1; Glasser et al., 2012), and could be expected to be contemporaneous. Detailed morphostratigraphic analyses are required to infer controls on glacier extent and glacier-glaciolacustrine interactions.

Our objectives are: (1) to constrain glacier extent and ice-dammed palaeolake dynamics using remote sensing and field mapping; (2) to date post-Last Glacial Maximum (LGM) readvances and the timing of palaeolake drainage events using ^{10}Be cosmogenic nuclide exposure ages from terminal and lateral moraines both above and below known lake levels; and (3) to evaluate the synchronicity of readvances during the Last Glacial Termination using our new geochronological datasets and previously published moraine ages.

2. Study area

2.1. Setting

Our study area is the Baker Valley region of the Andean Cordillera east of the NPI around 47°S (Fig. 1). Río Baker drains Lago General Carrera/Buenos Aires (Lago GCBA) and Lago Cochrane/Pueyrredón (Lago CP), and flows south of the NPI and into the Pacific Ocean. Ice dams across the Baker valley during the last glaciation resulted in the formation of large ice-dammed lakes east of the NPI. We focus on Soler Glacier, which currently drains east from the NPI and terminates on dry land. The glacier feeds a river, which flows into Lago Plomo, which is separated by a large moraine from Lago Bertrand. Lago Bertrand drains towards the Pacific via Río Baker (Fig. 1). During past glaciations, Soler Glacier blocked the drainage of Lago GCBA into Río Baker. We focus our attention on the Bertrand Moraines, deposited by Soler Glacier above 500 m asl, and therefore above the highest level of Lago GCBA. These moraines mark an advanced postion of Soler Glacier when it discharged into a deep ice-dammed palaeolake (Glasser and Jansson, 2008; Bendle et al., 2017a; Thorndycraft et al., 2018).

We also focus on the Salto valley, which was occupied by Calluqueo Glacier from MSL during past glaciations (Wenzens, 2002). Calluqueo Glacier deposited the Esmeralda and Salto moraines in this valley following recession from the LGM ice margin (Fig. 2). In contrast with the Bertrand Moraines, these moraines are at ~350 m asl, close to the elevation of an ice-dammed palaeolake.

MSL (47°35′S, 72°18′W; 3706 m high) is an isolated granodioritic to granitic massif (Ramos et al., 1982) on the eastern flank of the Andes (Figs. 1 and 2). It lies ~70 km east of the southern limit of the NPI (Sagredo et al., 2016). It sustains numerous small glaciers with an ice-covered area of 139 km^2. These glaciers are currently thinning (Falaschi et al., 2013, 2016). Calluqueo Glacier is the largest glacier (50.9 km^2) (Falaschi et al., 2016) (Fig. 2). Calluqueo Glacier and glaciers on the northern flank of the ice mass drain into Río Salto via the Salto and Tranquilo valleys. Río Salto enters Valle Grande at the Salto Waterfall, by the Salto Moraines, where it joins Río Baker and drains towards the Pacific (Figs. 1 and 2).

2.2. Past glacial history

Large outlet lobes from the NPI reached the Argentinian foothills during the LGM (Caldenius, 1932; Mercer, 1976; Hein et al., 2010; Coronato and Rabassa, 2011; Mendelova et al., 2017; Bendle et al., 2017a). The two most significant eastern outlet lobes of the NPI flowed out through Lago GCBA and Lago CP (Caldenius, 1932; Mercer, 1970; Douglass et al., 2006; Hein et al., 2010; Coronato and Rabassa, 2011; Smedley et al., 2016; Mendelova et al., 2017) (Fig. 1B). Outlet glaciers from MSL flowed southeast into Argentina in the Río Belgrano valley (Caldenius, 1932; Wenzens, 2003) and north into the Tranquilo and Salto valleys (Fig. 1), where they joined the larger Lago CP outlet lobe (Wenzens, 2002). Recession occurred rapidly after 17.7 ka (Bendle et al., 2017a). By the mid-Holocene, the ice masses had separated into disparate icefields centred on the main Andean mountain peaks, Lago Jeinemeni Reserve (Douglass et al., 2005) and MSL (Sagredo et al., 2016, 2018).

Following initial glacier recession after the LGM, ice-dammed lakes formed behind the moraines in the Lago GCBA and Lago CP valleys (Glasser et al., 2016). Geomorphic evidence for the lakes includes shorelines and stepped deltas, which suggest that the palaeolakes were stable before abrupt and rapid drops in lake level (Bell, 2008, 2009; Bourgois et al., 2016), caused by glacier recession opening up new drainage routes through lower elevation cols (Turner et al., 2005; Glasser et al., 2016). There are multiple competing models for ice-dammed palaeolake evolution (Turner et al., 2005; Bell, 2008, 2009; Hein et al., 2010; Bourgois et al., 2016; Glasser et al., 2016; Thorndycraft et al., 2018). It is generally agreed that, at their maximum heights, the ice-dammed palaeolakes drained eastwards towards the Atlantic. Drainage reversals occurred following ice recession, with the lakes ultimately reaching their current extent and draining westwards through Río Baker to the Pacific. These reconstructions used different names for different stages of palaeolake evolution, but have in common the reconstruction of a large, unified palaeolake at 340–350 m asl in the Cochrane and Lago GCBA valleys, which drained through the 350 m asl col at the head of Río Bayo north of Puerto Tranquilo (Fig. 1) (Glasser et al., 2016). We use “Lago Chalenko” when referring to the 350 m united ice-dammed lake (cf. Thorndycraft et al., 2018), which is the indigenous name for Lago GCBA. We term the highest level of Lago GCBA the “Deseado Level” (400 m asl), as at this time the lake flowed out through the Deseado col and through Río Deseado to the Atlantic.

2.3. Last glacial-interglacial transition in central Patagonia

The West Antarctic Ice Sheet Divide (WAIS Divide) ice cores indicate steady warming in the Southern Hemisphere from 18 ka, which was interrupted by the ACR cooling (Fudge et al., 2013; Wais Divide Project Members, 2015); warming continued in the Southern Hemisphere throughout the period of the Younger Dryas. Palaeoclimate studies from central Patagonia indentify the ACR as a cold period (Hajdas et al., 2003; Massaferro et al., 2014; Moreno and Videla, 2016). Villa-Martínez et al. (2012) recorded a cool climate

(2018). Published ages have been recalculated according to our protocols (Turner et al., 2005; Glasser et al., 2012; Villa-Martínez et al., 2012; Boex et al., 2013; Bourgois et al., 2016; Nimick et al., 2016; Sagredo et al., 2016, 2018). Glacier extent from Davies and Glasser (2012). Overlain on hillshaded ASTER GDEM. B. Chile, showing current icefields (black), from Davies and Glasser (2012), and extent of Patagonian Ice Sheet at LGM (light blue) (from Coronato and Rabassa, 2011). Red box shows extent of Map A. NPI: North Patagonian Icefield. SPI: South Patagonian Icefield. MSL: Monte San Lorenzo. (For interpretation of the references to colour in this figure legend, the reader is referred to the Web version of this article.)

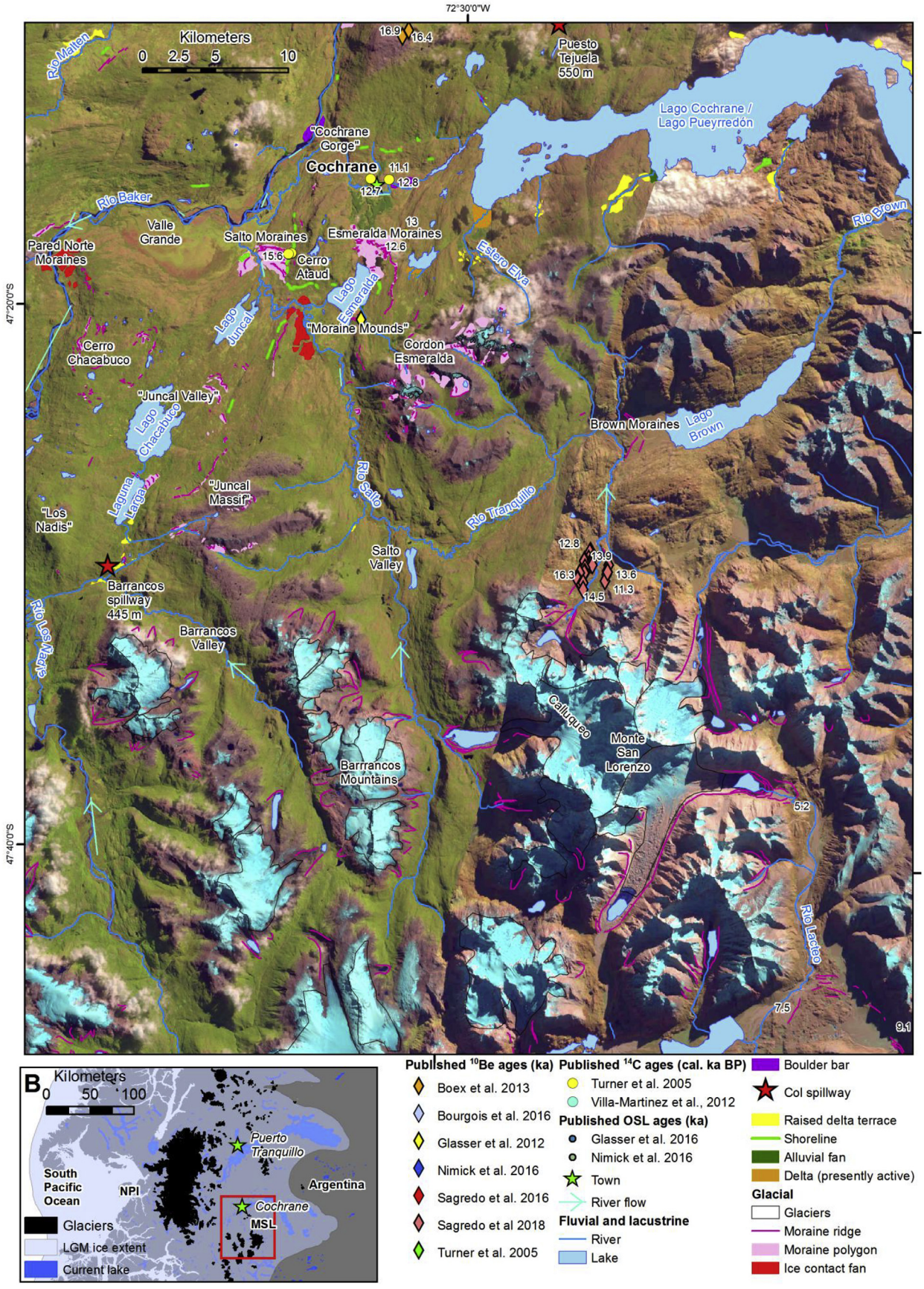

Fig. 2. Physiography of the Monte San Lorenzo (MSL) massif, showing the outlet glaciers of the mountain and the regional valleys.

with increased precipitation from 13.4 to 11.8 cal ka BP from Lago Augusta in the Chacabuco Valley (47°S). Palynological records from the nearby Lago Edita (Fig. 1) show increased precipitation between 14.5 and 13.0 cal ka BP (Henríquez et al., 2017).

The Younger Dryas (12.9–11.7 cal ka BP) was characterised by cooling in the North Atlantic (Lowe et al., 2008) and a slow-down in oceanic circulation (Lynch-Stieglitz et al., 2011). However, its expression in the Southern Hemisphere was less pronounced (Singer et al., 1998; Sugden et al., 2005; Douglass et al., 2006; Darvill et al., 2016). After 11.0 cal ka BP, palynological data from the Chacabuco Valley record declines in cold-resistant flora. A rise in *Northofagus* signal arboreal increase, warming and decreased precipitation (Henríquez et al., 2017).

3. Methods

We use a landsystems approach combined with cosmogenic nuclide dating. Systematic mapping allows landforms to be grouped into genetically linked sediment-landform assemblages, and the determination of a landsystem (Evans, 2005). Landforms were mapped in ESRI ArcGIS using ESRI Basemap World Imagery (usually Digital Globe and GeoEye images) and high resolution imagery from GoogleEarthPro. Elevation data were derived from ASTER GDEM (30 m resolution) (ASTER GDEM Validation Team et al., 2009). Slope and hillshaded elevation models were used to assist landform interpretation (Smith and Clark, 2005). Remotely sensed mapping was ground-truthed during fieldwork (November–December 2015, December 2016, December 2017). Field mapping utilised a handheld GPS (accurate to ± 8 m) and followed standard procedures (Smith et al., 2011; Otto and Smith, 2013). Moraine transects were conducted using a hand held GPS, an Abney level and tape measure to measure distance and angle to breaks in slope. Large transects were calculated in ArcGIS using ASTER GDEM. Regional landscape mapping built on published geomorphological maps (Turner et al., 2005; Glasser and Jansson, 2008; Bendle et al., 2017b; Thorndycraft et al., 2018). In places, dense forest and steep, unstable slopes precluded mapping.

Glacially transported boulders with abundant quartz situated on moraine ridge crests were targeted for ^{10}Be exposure-age dating. Rock samples were collected following standard guidelines (Gosse and Phillips, 2001; Cockburn and Summerfield, 2004; Balco, 2011; Darvill, 2013). Where possible, ≥5 boulder samples were sampled per moraine ridge (cf. Putkonen and Swanson, 2003; Cockburn and Summerfield, 2004). We targeted boulders with a >1 m *b* axis that were raised well above the local ground surface (cf. Putkonen and Swanson, 2003; Heyman et al., 2016) with signs of glacial erosion (e.g., edge-rounding, faceting), avoiding angular boulders that may have been transported supraglacially, boulders that were very weathered or flaking, or those that may have rolled or been exhumed. Samples (<5 cm thick and weighing >1 kg) were taken using a hammer and chisel (thus minimising environmental impact by making a smaller, more subtle indentation compared with other methods using rock saws) from the centre of the flat top surface of the boulders, away from cracks, edges and joints. Detailed sample descriptions are provided in the Supplementary Information.

Samples were processed for cosmogenic ^{10}Be analysis at the SUERC Cosmogenic Isotope Laboratory. Samples were crushed and sieved to 250–500 μm and quartz was separated in a Frantz® isodynamic magnetic mineral separator before being repeatedly etched in 2% HF until 30% of the quartz mass was lost (Kohl and Nishiizumi, 1992). Quartz purity was assayed by ICP-OES. Purified quartz was spiked with ~0.23 mg of ^{9}Be and dissolved. Beryllium was extracted and isolated following the methodology described in Child et al. (2000) before being precipitated as $Be(OH)_2$ and baked to BeO in a quartz crucible. BeO was mixed with Nb and pressed into a copper cathode. Cosmogenic nuclide concentrations include a procedural blank correction of 50,751 ± 11,188 atoms (^{10}Be/^{9}Be = $3.35 \times 10^{-15} \pm 7.37 \times 10^{-16}$). ^{10}Be/^{9}Be was measured using the 5MW pelletron at SUERC (Xu et al., 2010) and normalised to NIST SRM4325 with a ^{10}Be/^{9}Be ratio of 2.79×10^{-11} (Nishiizumi et al., 2007). Cosmogenic nuclide concentrations include a procedural blank correction of 50,751 ± 11,188 atoms. The uncertainties in the cosmogenic nuclide concentrations include the AMS counting statistics and scatter uncertainties from sample, procedural blank, and standards measurements.

The ages were calculated using the CRONUS-Earth online calculator (Balco et al., 2008), version 2.3 (wrapper script 2.3; main calculator 2.1; constants 2.3; muons 1.1), with a local Patagonian production rate of 3.88 ± 0.15 atom/g/yr derived from the calibration data set of Kaplan et al. (2011) from the ICE-D online database (http://calibration.ice-d.org/), the time-varying Lm scaling method (Lal, 1991; Stone, 2000), and a rock density of 2.7 g/cm^3. We applied a correction for topographic shielding using measurements of the horizon line conducted in the field. As erosion rates are poorly constrained regionally we use an erosion rate of 0 mm/kyr, but also provide ages with 1 mm/kyr erosion rates for comparison. The choice of erosion rate leads to little difference on boulder exposure ages within the timescale of this study, since the difference in calculated age is smaller than the calculated uncertainties. We include no correction for periodic snow cover, which is likely to be negligible in this windy setting and given the size of boulders sampled. No correction for post-glacial uplift has been applied. Published regional exposure ages are recalculated using our protocols. Cosmogenic and optically stimulated luminescence (OSL) ages are presented as "ka".

Normal kernel density estimates ("camel plots") are used to visually evaluate the ages and identify outliers. Code to generate these plots was created in Matplotlib, modified from Balco (2009). Outliers due to isotope inheritance are usually easily identified; however, incomplete exposure biases such as erosion, weathering, rolling, exhumation or burial may not produce obvious outliers, since these processes are differential. Boulder ages may therefore underestimate the timing of moraine formation (Briner et al., 2005; Heyman et al., 2016). However, an 'oldest boulder' approach (cf. Putkonen and Swanson, 2003) is also potentially an over simplification of a complex dataset. We use uncertainty weighted means (UWM) and kernel density plots to evaluate our dataset, since these approaches take into account the range and distribution of ages on a moraine once clear outliers are excluded.

Published radiocarbon ages were recalibrated using CALIB and the SHCal13 dataset (Stuiver et al., 2009; Hogg et al., 2013), and the calibrated mean ages (2σ) are presented as "cal. ka BP" (Reimer et al., 2013).

4. Salto Valley geomorphology

4.1. Glacial landforms

4.1.1. Lateral moraines

There are three sets of sloping, sharp-crested lateral moraines (field checked at 380 m, 510 m and 710 m asl) on the north-western flank of Cordon Esmeralda (Figs. 3–6). The 510 m lateral moraine is contiguous with the Esmeralda Moraines (Fig. 4). We did not identify a contiguous terminal moraine with the 710 m lateral moraine (located directly above the Esmeralda Moraine), suggesting that the higher-level glacier was confluent with Colonia ice in the main valley.

Lateral moraines in Baker Valley wrap around Cerro Chacabuco into "Juncal Valley" at 650 m asl, dropping to 400 m asl near the Pared Norte Moraines (Fig. 3). On the side of Juncal Massif, there are

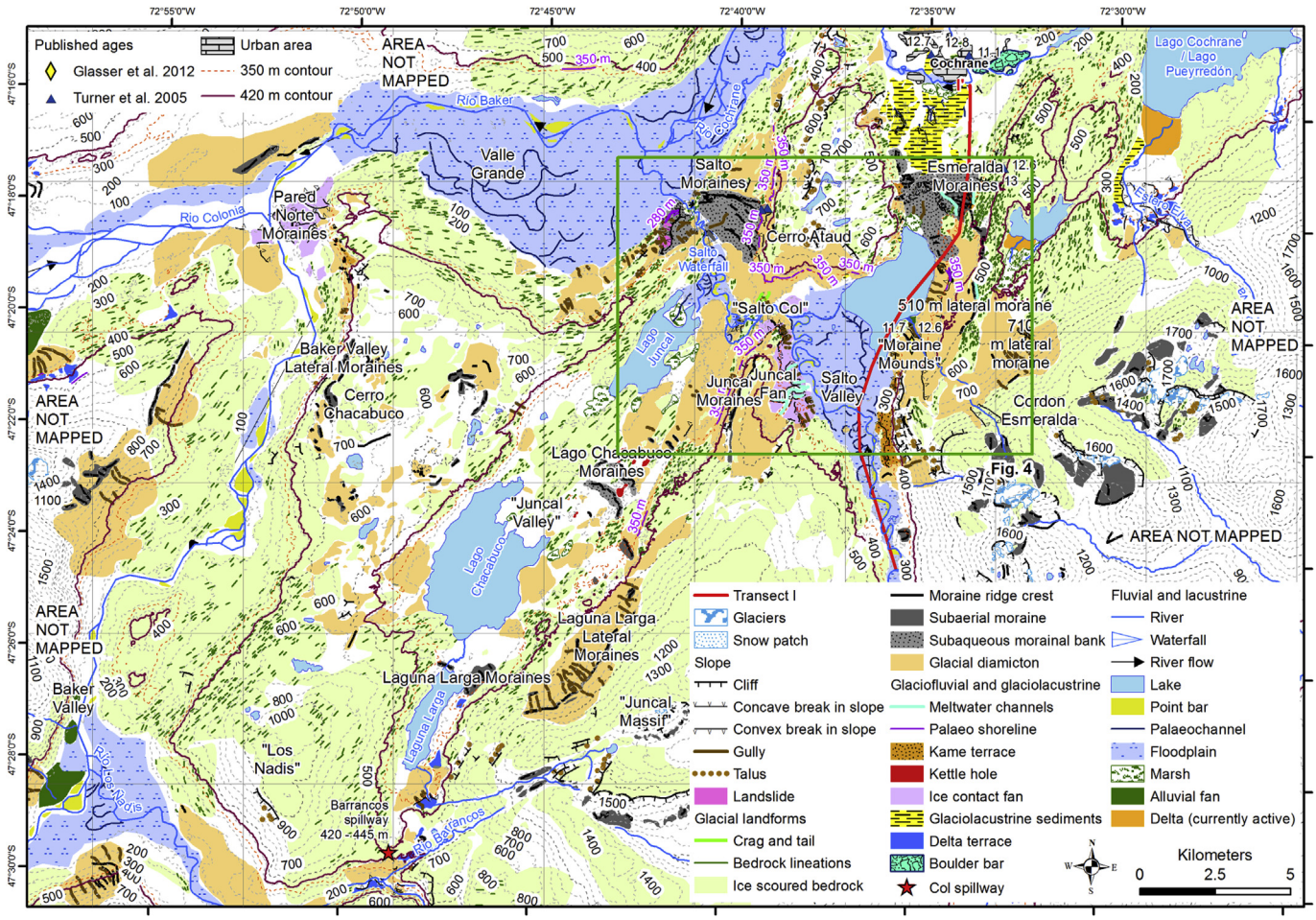

Fig. 3. Geomorphological map of the Esmeralda and Salto moraines in the Salto Valley, and the Juncal moraines in the Juncal Valley. Grid spacing: 5 km. Location of boulder bars and deltas after Thorndycraft et al. (2018). Contours from ASTER GDEM. Location of Fig. 4 is indicated by the green box. See Fig. 1 for overall situation. (For interpretation of the references to colour in this figure legend, the reader is referred to the Web version of this article.)

lateral moraines above Laguna Larga and Lago Chacabuco at 800 m asl. They are contiguous with the Juncal Moraines (555 m asl) further down the Juncal Valley, above Lago Juncal (Fig. 3).

4.1.2. Subaerial moraines

The Esmeralda moraines (Figs. 3 and 4) comprise two clear sets of moraines on the western and eastern sides of the valley respectively, separated by a deep channel. Those moraines on the east of the channel ("Esmeralda Moraines" on Fig. 4) comprise a clear cross-valley, sharp-crested and arcuate ridge crest at 360–366 m asl, which was sampled for cosmogenic nuclide dating (see Section 6). The ridge is *ca.* 3 m wide at the crest, 60 m high, with symmetrical proximal and distal slopes both 30° steep (Fig. 6A and B; profiles E and C in Fig. 5). Inside the main ridge crest, several inset smaller latero-terminal moraines record subsequent glacier recession (Figs. 4 and 6C). The surficial sediments comprise a silty-sandy diamicton with numerous erratic cobbles and boulders.

At the distal foot of the moraines are bedded gravelly sands, which grade to well-sorted laminated silty clays (Section 4.2.1) in the basin downstream in the valley. Palaeoshorelines etched onto the hillside in front of and behind the moraines, but below their crestline, indicate that a palaeolake was extant both during moraine formation and following glacier recession.

We interpret these moraines as subaerial push moraines (Bennett, 2001). Similar push moraines in association with glacial lakes have been noted in Iceland (Bennett et al., 2000). A subaerial interpretation precludes any lakes higher than the crest of the moraine (366 m asl) at the time of moraine emplacement, which is in agreement with the lack of deltas or shorelines higher than 350 m asl in this locality. We suggest that the narrower, confined nature of the valley and higher elevation of the bedrock focused sediment delivery, leading to the formation of a higher push moraine where subaerial processes dominated.

The Esmeralda terminal subaerial push moraine links continuously with the 510 m lateral moraine, indicating an ice source from MSL, rather than the NPI, as has previously been suggested (Glasser et al., 2012, 2016). We call this "Calluqueo Glacier". South of the Esmeralda Moraines are the "Moraine Mounds", originally mapped by Glasser et al. (2012) (Fig. 4). They comprise prominent ridges running towards a bedrock high at the lake edge, with hummocky, morainic topography on the ice-proximal side. Granite boulders from their crest yielded exposure ages of 11.7 ± 0.6 and 12.6 ± 0.9 ka (Glasser et al., 2012). They represent a stillstand during the recession of Calluqueo Glacier.

4.2. Glaciolacustrine landforms

4.2.1. Laminated silts and clays

North of the Esmeralda moraines are glaciolacustrine sediments (Bendle et al., 2017b) (Fig. 3) comprising well sorted, laminated silts

and clays (Fig. 7A) with dropstones. They form a well-vegetated area of upstanding relief downstream of the Lago Esmeralda moraines, dissected by palaeochannels and Río Cochrane. Close to the moraines, fans fine upwards from cobbles to silty sediments whilst near Cochrane, laminated silts and clays (some with varve appearance) crop out at elevations of 170–200 m. These sediments were deposited by sediment-laden glacial meltwater entering the lake environment, where they were affected by gravity. The underflows moved away from the ice margin towards topographic lows, with sediment being deposited as momentum was lost (cf. Ashley, 2002). Studies from contemporary glacial lakes in Patagonia have emphasised the importance of underflows in these environments, since water density is controlled by suspended sediment concentrations rather than by water temperature or salinity, as is the case in glaciomarine fjords (Sugiyama et al., 2016). Rhythmic parallel laminated sediments such as these are characteristic of lake environments with sediments deposited by underflows (Ashley, 2002; Carrivick and Tweed, 2013).

4.2.2. Deltas

A series of flat-topped delta terraces are present beyond the Esmeralda moraines, at 350–460 m asl at the foot of Río Estero Elva, which drains into Lago CP (Fig. 3), and at 150 m asl, superimposed on the Salto Moraines (Fig. 8A). Gilbert-type deltas form where streams enter lakes (Ashley, 2002; Longhitano, 2008; Bell, 2009; Slaymaker, 2011; Dietrich et al., 2017). They often form in stepped sequences upstream of modern and actively forming lake deltas (Bendle et al., 2017b). These ice-distal glaciolacustrine deltas were fed by a fluvial network issued from the retreating ice margin (cf. Dietrich et al., 2017).

4.2.3. Palaeoshorelines

Palaeoshorelines are eroded into the diamictic sediments on the hillsides both north of Cochrane at 460 m asl (Fig. 3), and consistently at: 340–350 m asl in Valle Grande; around the Juncal Massif (Fig. 7B); inside the Esmeralda moraines (Fig. 4); and around the southern and western margin of Cerro Ataud, where they are associated with the Salto moraines (Fig. 8B). Shorelines are also cut into the ice-distal face of the Salto Moraine at 280 m asl (Fig. 4; Fig. 8A). The shorelines take the form of a gently valley-dipping platform (e.g. Fig. 7B) with a flat long profile, and frequently bear exotic and local boulders. These erosional features, backed by cliffs, are similar to features observed in other parts of Patagonia (Bentley et al., 2005; Glasser et al., 2009; García et al., 2014).

These palaeoshorelines constrain the evolution of ice-dammed lakes in the region. The higher ~460 m asl shoreline is located to the north of Cochrane whilst the ~350 m asl shorelines extend into the Salto and Juncal valleys. In tandem with the glacial geomorphology (Section 4.1), this demonstrates that Esmeralda moraine formation was coeval with the 350 m asl palaeolake in this valley.

4.2.4. Morainal banks

Asymmetric moraines closely associated with the 350 m asl

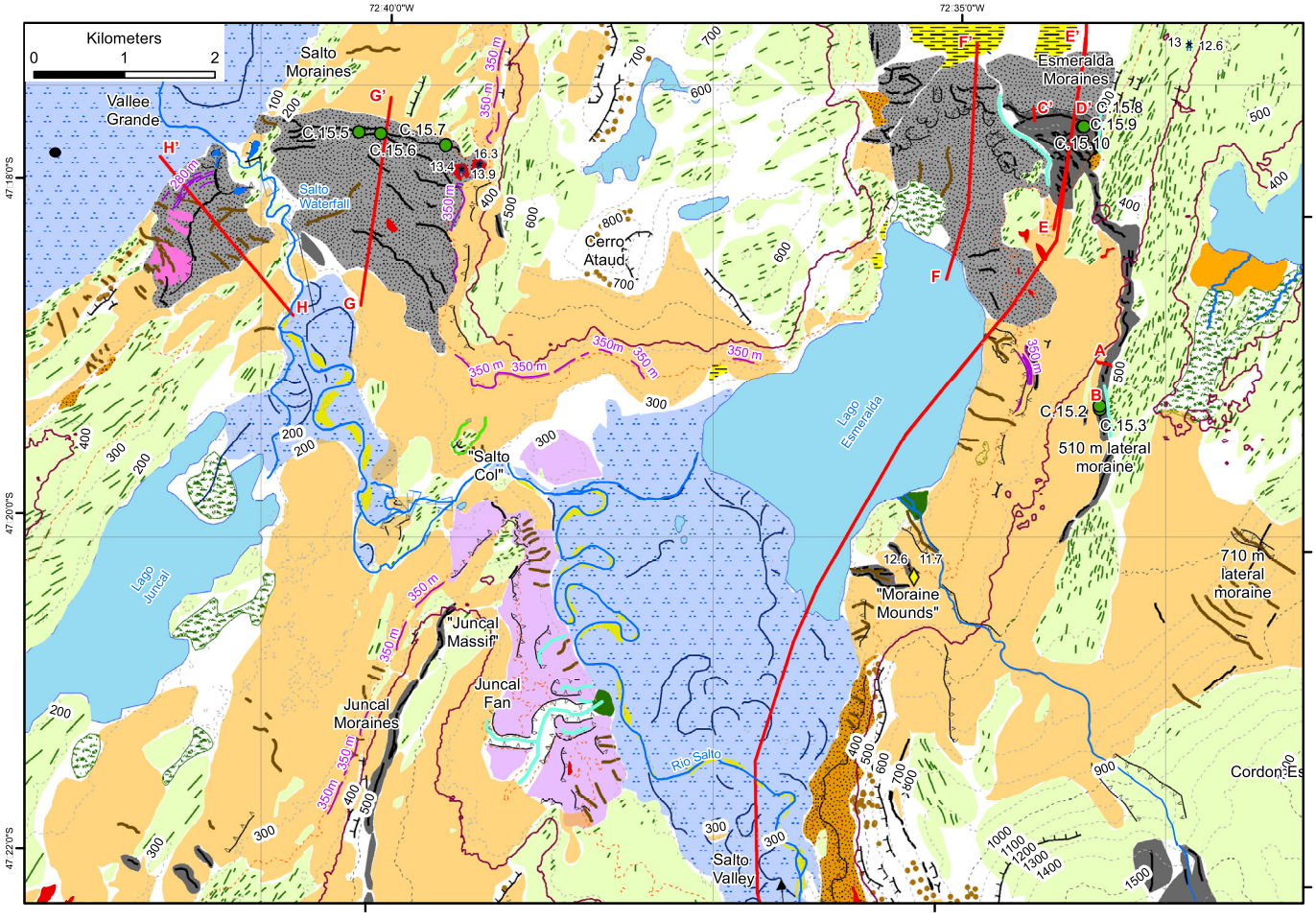

Fig. 4. Detailed map of Esmeralda and Salto moraines, showing location of samples and moraine transects. Transect "I" is shown in Fig. 3. Grid spacing is 5 km. Green circles are cosmogenic nuclide samples. Legend as in Fig. 3. (For interpretation of the references to colour in this figure legend, the reader is referred to the Web version of this article.)

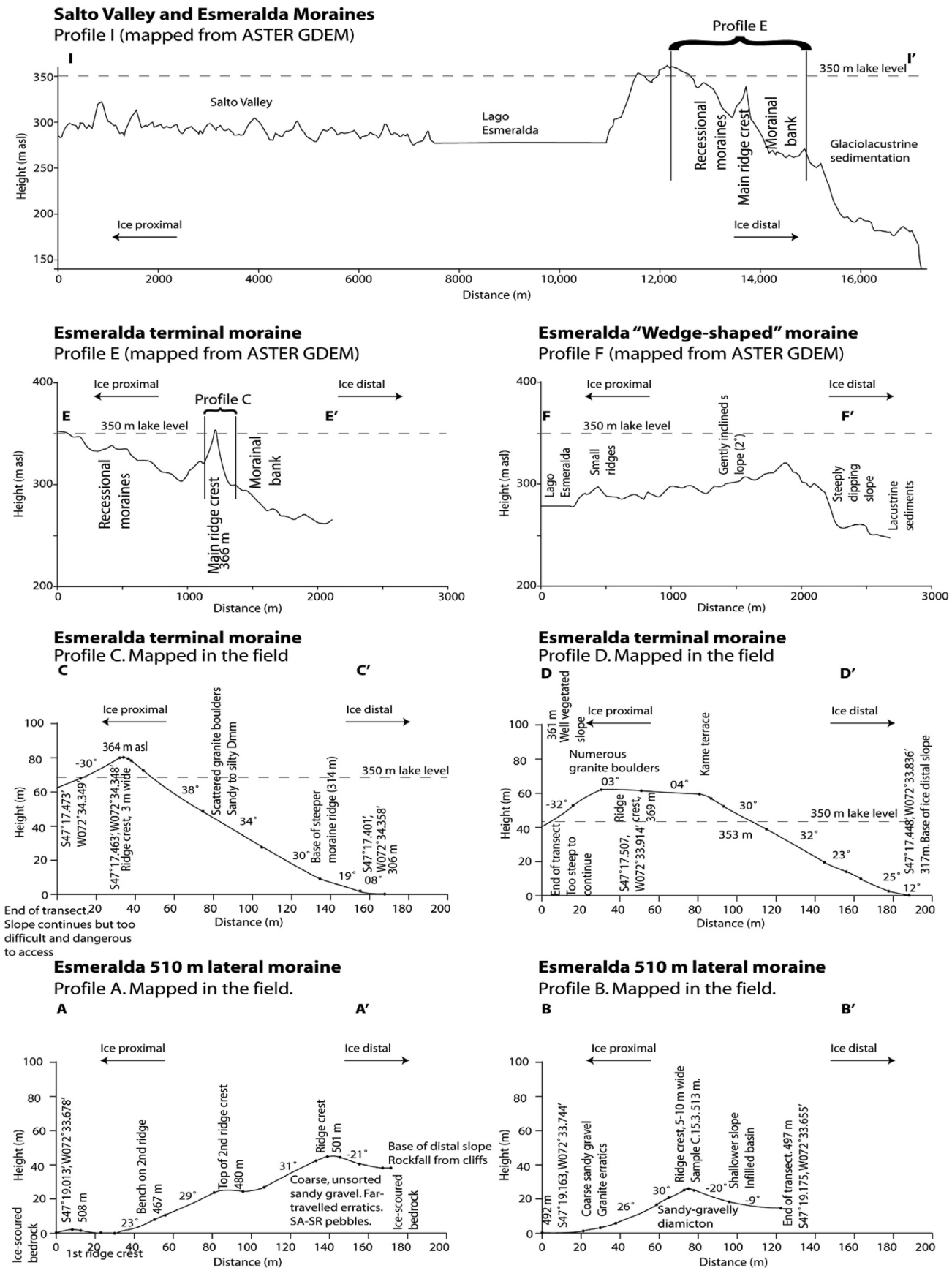

Fig. 5. Cross profiles of the Salto Valley and Esmeralda moraines. Transects are shown on Fig. 3 and 4. Note that the narrow ridge crest in profiles I and E is not well captured by the coarse resolution of the ASTER GDEM.

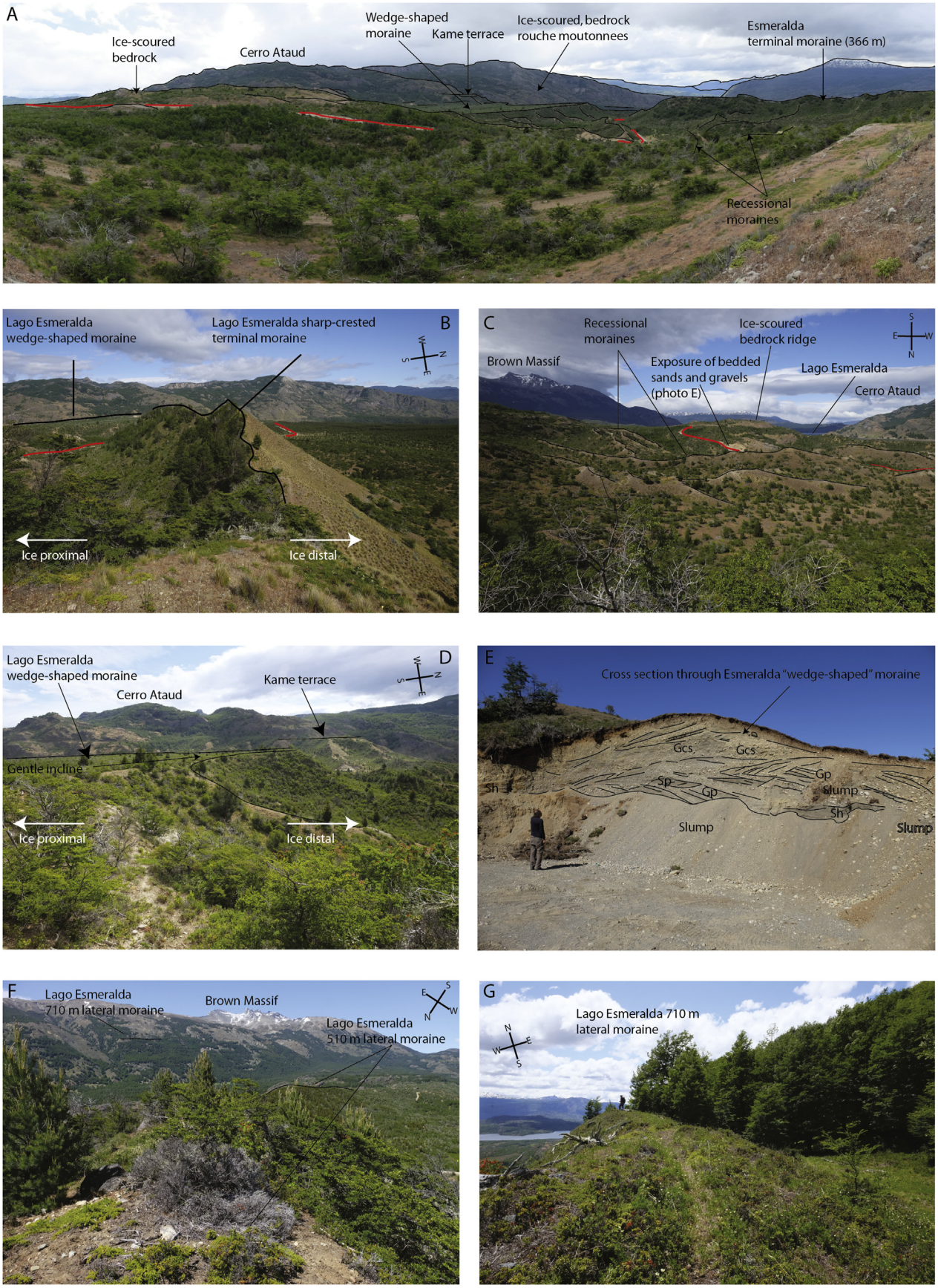

Fig. 6. Representative photographs of the Esmeralda moraines. Red lines indicate roads. A. Overview of the Esmeralda moraine complex. B. Esmeralda terminal sharp-crested push moraine. C. Recessional moraines behind the main ridge crest depicted in B. D. Esmeralda wedge-shaped moraine, showing horse-shoe shaped scars and 360 m kame terrace. E. Exposure in the wedge-shaped morainal bank. F. Esmeralda 510 m moraine. G. Esmeralda 710 m lateral moraine. Lithofacies codes after Evans and Benn (2004). (For interpretation of the references to colour in this figure legend, the reader is referred to the Web version of this article.)

palaeolake shorelines are found in the Salto and Juncal valleys. Adjacent to the sharp-crested Esmeralda Moraine there is a wedge-shaped moraine rising to 330 m asl dips back towards Lago Esmeralda at 2° over 2 km (Figs. 4 and 6A, D; profile F in Fig. 5). The distal slope dips at 30° towards Cochrane and is marked by numerous horse-shoe shaped crescentic scars (Fig. 4; Fig. 6D). Exposures reveal a silty, stone-rich, massive diamicton and interbedded trough cross-bedded sands and gravels (Fig. 6E).

The Salto Moraines, which reach heights of up to 350 m asl, are at the edge of a hanging valley, perched above Valle Grande (Fig. 8). The northern Salto Moraines are sharp-crested at their north-western flank, near Valle Grande, but as they near Cerro Ataud the ice-proximal face becomes more gradual, and slopes gently inland towards Lago Juncal over a distance of some 1.7 km (Fig. 8B; Profile G in Figs. 4 and 9). The ice distal slope is steep and well defined (Fig. 9, Fig. 8C and D). The gentle ice-proximal slope is interrupted with multiple small recessional moraines. Small exposures of surficial sediments in the ridges reveal a silty, stone-rich diamicton. Where the Northern Salto Moraines meet Cerro Ataud, they are cut by shorelines at 350 m (Fig. 4; Fig. 8B). Outside and north of the moraines, the shoreline is ~50 m wide, littered with locally derived angular gneiss boulders and rounded to sub-rounded granite clasts (Fig. 8D, E, F), indicative of local talus input.

In the "Juncal Valley", the "Lago Chacabuco Moraines" and "Laguna Larga Moraines" (Fig. 3) have a similar asymmetric profile to the Salto Moraines, with a shallow ice-proximal slope and a steep ice-distal slope. Between the moraine crests are several infilled kettle holes.

We interpret all these landforms as subaqueous morainal banks (cf. Glen, 1954; Rovey and Borucki, 1995; Turner et al., 2005; Batchelor and Dowdeswell, 2015; Bennett et al., 2000) deposited by a valley glacier terminating in water. Following glacier recession from Valle Grande, the glacier that deposited the Salto Moraines was left as a hanging valley with a morainal bank at its mouth. As ice receded from Valle Grande, Lago Chalenko extended into the valley. Lago Chalenko drained through the 350 m col at Rio Bayo, and the lake was therefore confluent in the Lago GCBA and Lago CP valleys (Glasser et al., 2016). Both the Salto (Fig. 8) and Esmeralda

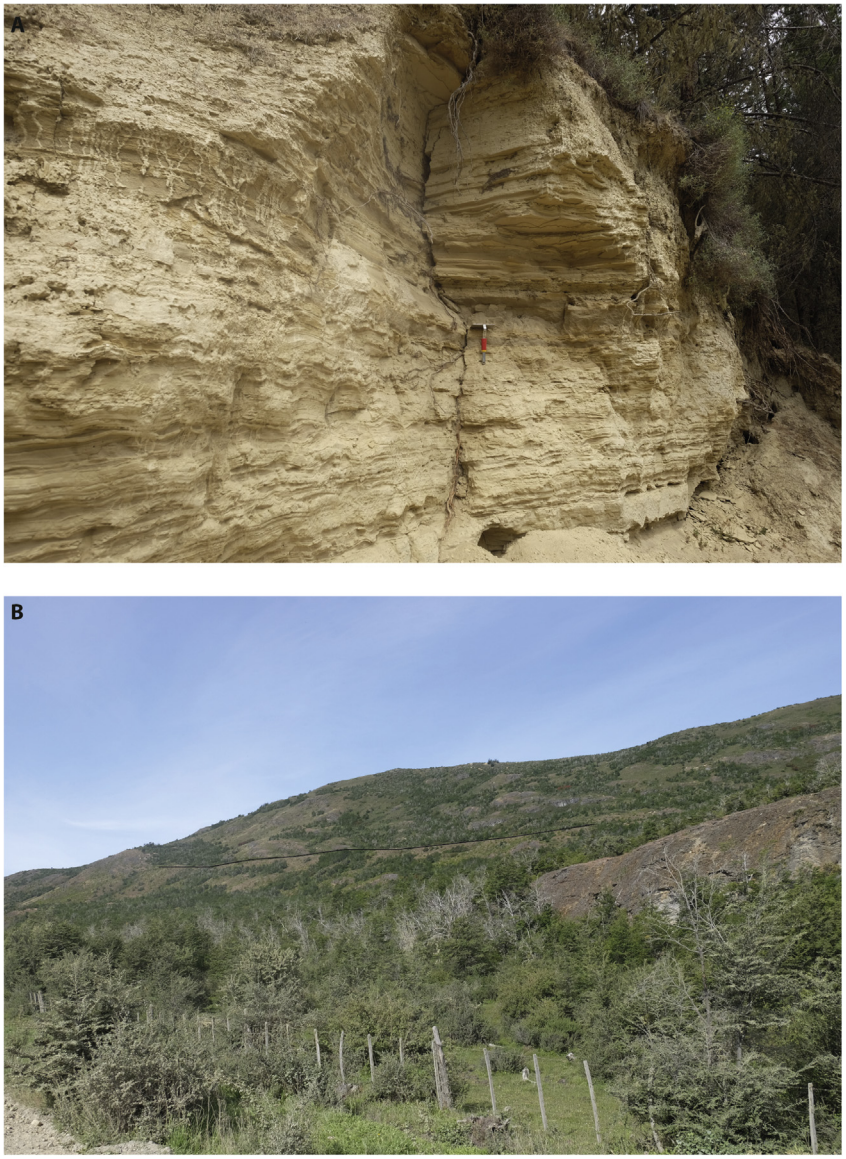

Fig. 7. Glaciolacustrine sediments and landforms. A. Laminated glaciolacustrine silty clays in the basin downstream of the Esmeralda Moraines. B. 350 m asl palaeoshoreline (highlighted with arrows) and ice-sculpted bedrock in Juncal Valley.

Fig. 8. Representative photographs of the Salto Moraines. A. View over Valle Grande and Río Baker, with the Western Salto Moraines and delta terraces highlighted. B. View of the northern Salto Moraines, showing the ridge crest and prominent 350 m shoreline. C. View of the ice-distal slope of the northern Salto Moraines. Note the steep slope. D. View of the ice-distal slope of the Salto Moraines, showing the gradual incline of the ice-proximal slope. Juncal Moraines are visible in the middle distance, and Monte San Lorenzo is visible in the far distance. E, F. Close view of the ridge crest of the Northern Salto Moraines, with scattered granite boulders.

moraines (Fig. 5, profile I) are positioned at bedrock highs, where the glacier would have entered deeper water, indicating that stabilisation of the ice margin was at least partly controlled by topography and calving dynamics.

Lateral moraines indicate that the Lago Chacabuco and Laguna Larga moraines were formed by a glacier that flowed from the Barrancos Mountains, down Barrancos Valley and into Juncal Valley. We call this the "Barrancos Glacier". Shorelines and deltas indicate that the valley was flooded by the 350 m Lago Chalenko following glacier recession. The glacier was likely confluent with ice forming the Salto moraines from the Salto Valley, before receding to the Juncal Valley before the 350 m palaeolake drained, resulting in shorelines being imprinted over the moraines.

4.2.5. Ice-contact fans

On the eastern flank of "Juncal Massif" an accumulation of sediments dips gently towards the valley floor (Fig. 4). The slope of the terrace is steeply incised by numerous gullies and meltwater channels, the largest of which has an abandoned alluvial fan at its base (Fig. 4). The top of the terrace reaches ~380 m asl. A rounded break in slope occurs at 365 to 330 m asl. The top surface is ~30 m wide, and dips at ~10°–17° towards the valley floor. After the break in slope, it steepens to 20°–25°. Exposures in road cuttings show that the sediments of this terrace comprise a stone-rich diamicton with a silty sandy matrix and with abundant fine to coarse gravel. The diamicton is overlain by stratified, poorly sorted, clast-supported sandy gravels with a silty sand matrix.

We interpret the gently sloping top surface of the Juncal Fan as a kame terrace. The more steeply dipping slope (20°) is interpreted as a subaqueous ice-contact fan, imprinted on top of the kame terrace following glacier recession. Ice-contact fans are sloping sediment accumulations that form subaqueously at the grounding line of glaciers (Powell, 1990; Winsemann et al., 2009; Dowdeswell and Vásquez, 2013; Lønne, 1995; Boston and Lukas, 2017). These landforms form at the grounding line when sediment-laden meltwater is released from the glacier as an efflux jet into a glacial lake (Lang and Winsemann, 2013). These high-energy flows build a fan-shaped sediment accumulation. The break in slope on the Juncal Fan is contiguous with the 350 m shoreline in the Juncal Valley, providing a clear stratigraphic association with the 350 m Lago Chalenko.

5. Lago Bertrand geomorphology

5.1. Glacial landforms

A series of moraines on the northern hillside above Lago Bertrand (Fig. 10) were deposited by an advanced Soler Glacier. The Bertrand moraine chronology is also reported by Thorndycraft et al. (2018), where the timing of moraine deposition is used to define a maximum age for Soler Glacier ice blocking Río Baker drainage. Here we provide the first detailed glacial landsystem analysis of the site, and interpret the glaciological significance of the ages.

Above Lago Bertrand there are four sets of moraines (LBM1 to 4 that we term the Lago Bertrand Moraine Complex (LBMC); Fig. 11). The moraines are located above the limits of the 11 ka Plomo and Lago Negro moraines (Fig. 10) (cf. Glasser et al., 2012), with LBM4, the most northerly and most extensive lobe situated at the col between the Lago Bertrand and Río Canal valleys (Fig. 10; Fig. 11).

LBM1 moraines extend from 490 to 550 m asl (Fig. 11). The ridge crest runs parallel to the slope towards Lago GCBA. Numerous large rounded granite boulders are visible just south of the ridge, but none are visible north of the ridge, where the local gneiss bedrock is ice-scoured with streamlined roche moutonnées. LBM1 traces round to LBM2. The more substantial LBM2 moraines reach up to 640 m asl, and are interspersed with small kettle holes, and are situated at the top of a valley, indicating a glacier that flowed up a reverse-bed slope (Fig. 11; Fig. 12A). The moraine ridges themselves

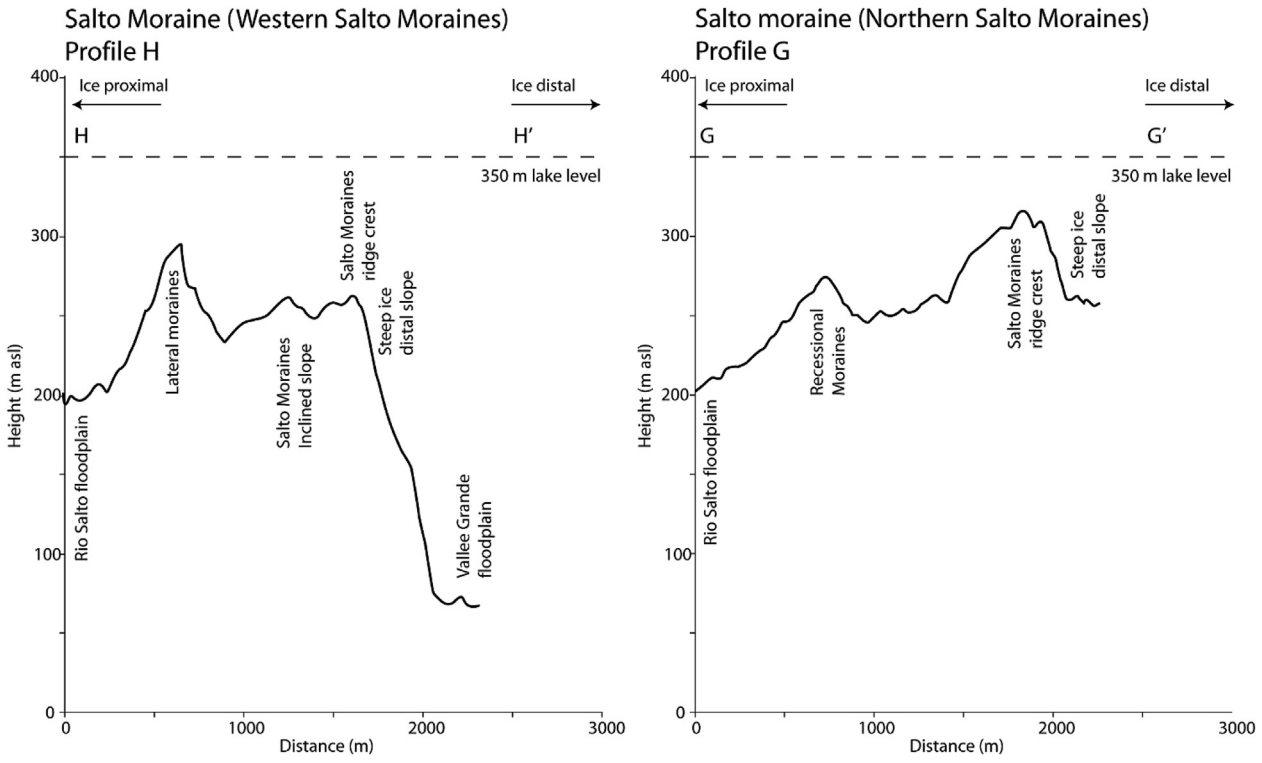

Fig. 9. Cross profiles of the Salto Moraines, derived from ASTER GDEM. For location of profiles see Fig. 4.

are up to 100 m above the narrow valley floor, with numerous large erratic granite boulders on the crestline (Figs. 11 and 12A, B, D). Ice-scoured gneiss prevails beyond the moraines (Fig. 11).

LBM3 comprises an inner and an outer crescent-shaped moraine (Fig. 12C, E), both of which wrap around an approximately circular lake (Fig. 12C). The arcuate ridges are ~10–20 m high and are steep-sided and sharp-crested. Although these moraines are located up-ice, they are lower, reaching 575 m asl (LBM3 inner moraine) and 555–566 m asl (LBM3 outer moraine). Kettle holes are present between and beyond the moraines.

LBM4 moraines are located further northwest at ~550 m asl, with a lateral moraine extending up to at least 700 m asl into the Bertrand valley. They comprise chaotic, discontinuous mounds interspersed with meltwater channels. Large numbers of locally derived angular gneiss boulders are at the terminus of these moraines, suggesting a rockfall event onto the glacier surface (the moraines are not directly overlooked by steep cliffs that could produce these rocks). The arrangement of the moraine crests suggests that LBM4 predate LBM3.

These diamictic, arcuate moraines, interspersed with infilled kettle holes between moraine ridge crests, are typical of active-temperate glaciers (Evans, 2003; Evans et al., 2006). The moraines of the LBMC are formed on reverse-bed slopes and represent small protrusions extending laterally from a large trunk glacier that filled the Lago Bertrand valley (Soler Glacier). LBM1 represents the lateral moraine near the terminus of the glacier at Bertrand col. The moraines record a period of glacier thinning. LBM1, 2 and 4 represent the oldest and highest moraines, when ice was presumably flowing over the col into the Río Canal valley. Thinning ice resulted in recession from LBM2 and the formation of LBM3, with the close-set inner and outer moraines pf the latter likely representing just a small step back of the glacier.

As ice flow is driven by ice-surface slope (Cuffey and Paterson, 2010), we infer that the thickest recorded ice surface (Soler Glacier) in Lago Bertrand at this time was >640 m asl at the location of the LBMC. Given that Lago Bertrand is ~90 m deep, this indicates an ice thickness >730 m near the eastern end of Lago Bertrand.

5.2. Glaciolacustrine landforms

5.2.1. Ice contact fans

LBM1 moraines trace the ice margin down to the terminus position at the boundary col between Lago Bertrand and Lago GCBA, where there is a thick accumulation of diamicton (Fig. 11). It is incised by a shoreline at 345 m asl. The diamicton grades into a flat-topped ice-contact fan at 300 m asl (Fig. 11), formed subaqueously at the terminus of Soler Glacier (Thorndycraft et al., 2018). This feature has previously been described as a moraine (Bourgois et al., 2016) with a single, outlying, cosmogenic nuclide exposure age of 17.5 ± 4.1 ka (at 299 m asl).

5.2.2. Delta terraces and shorelines

Raised deltas and palaeoshorelines around the edge of Lago GCBA include a flight of strandlines from 201 m (the current lake level) to 415 ± 5 m at the eastern end of Lago GCBA (Bourgois et al., 2016). Shorelines are incised into glacial diamicton at 440 m asl near LBM 3, and at 340 m asl through the LBM 1 moraines (Fig. 11). Stepped deltas associated with Río Las Dunas and Río Los Maitenes range from 320 to 650 m asl (Bell, 2009) (Fig. 10), although the highest two were reinterpreted as river terraces (Bourgois et al., 2016) or small ice marginal lakes (Martinod et al., 2016).

These data indicate the presence of a palaeolake at 400–440 m asl (Bell, 2008, 2009; Glasser et al., 2016). The variance in height is due to the differential isostatic rebound at the near and far ends of the lake (Turner et al., 2005; Thorndycraft et al., 2018). This indicates that when Soler Glacier terminated at Bertrand col and formed the LBMC, it calved into the 400 m "Deseado" Lago GCBA. At this time, the glacier dammed drainage south through Río Baker and prevented the formation of a unified ice-dammed lake through the Baker valley.

Evidence of the unified 350 m Lago Chalenko includes a raised delta terrace at 340 m asl at the mouth of the Río Canal valley to the north, and a shoreline superimposed on LBM1 at 345 m asl (Fig. 11). Deltas at 350 m asl are also present above the present-day Lago Bertrand, indicating that Soler Glacier had receded as far as the Plomo Moraine (dated to 10.6 ka; Glasser et al., 2012) at the time that the 350 m Lago Chalenko formed in the Baker, Chacabuco, Lago GCBA and Lago CP valleys (cf. Thorndycraft et al., 2018).

6. Chronostratigraphy

6.1. Esmeralda and Salto Moraine chronology

We collected eight samples for ^{10}Be cosmogenic nuclide exposure-age dating (Table 1 and Supplementary Fig. 1) comprising five samples from the contiguous Esmeralda lateral (510 m asl)/terminal moraine complex (365 m asl) and three from the Salto Moraines (338–359 m asl). Given the morphostratigraphic relationship of the Esmeralda and Salto moraines to the 350 m shoreline and the geomorphic evidence suggesting the moraines are subaerial/subaqueous, described above, all the boulders from the Esmeralda moraines were located above palaeolake Chalenko, whilst two of the boulders from the Salto Moraines were below the palaeolake, and one just above. The Esmeralda Moraine ages range from 13.3 ± 0.5 to 12.8 ± 0.6 ka. The ages of the two Salto Moraine boulders below the 350 m shoreline are 12.1 ± 0.4 to 12.0 ± 0.4 ka, and one boulder above the shoreline yielded an age of 12.5 ± 0.4 ka; therefore all the boulder exposure ages from the Salto Moraine are within errors of each other (see Table 2).

Fig. 13 shows normal kernel density estimate plots, with each age plotted as an individual Gaussian curve using internal uncertainties, for both our ages (Tables 1 and 3) and published ages. The samples from the contiguous and subaerial Esmeralda 510 m lateral and terminal moraines are well clustered, with no outliers (Table 1, Fig. 13), so we calculate the external uncertainty-weighted mean (UWM) age from these moraines together as 13.0 ± 0.6 ka. The UWM of the Moraine Mounds (cf. Glasser et al., 2012) is 12.1 ± 0.6 ka.

The UWM of the two exposure ages from the Salto Moraines that are below the 350 m shoreline is 12.1 ± 0.5 ka (Table 1), likely dating the timing of lake-level fall. Seasonal water-level variations are unlikely as lake depth is controlled by the height of the col (Bayo col at 350 m asl; Glasser et al., 2016). Water shields boulders from cosmic rays in the same way as ice and any other matter (Schaller et al., 2002; Fabel et al., 2010; Balco, 2014; Small and Fabel, 2015); 26 m of water has the same shielding effect as 10 m of granite. Sampling boulders from this morainal bank, which were only exposed when the lake drained, provides a minimum age for lake drainage. In general, samples above the lake water at the Salto and Esmeralda limits together indicate an advance of Calluqueo Glacier from MSL during the later part of the ACR, with palaeolake drainage at ca. 12 ka, when the ice margin was near the Moraine Mounds.

6.2. Lago Bertrand moraine complex (LBMC) chronology

The LBMC (Fig. 11) ages constrain an advance of Soler Glacier into Bertrand Valley, where it calved into the 400 m Deseado level of Lago GCBA at Bertrand col. All of these moraines are above the level of any mapped palaeolake in this region (Turner et al., 2005;

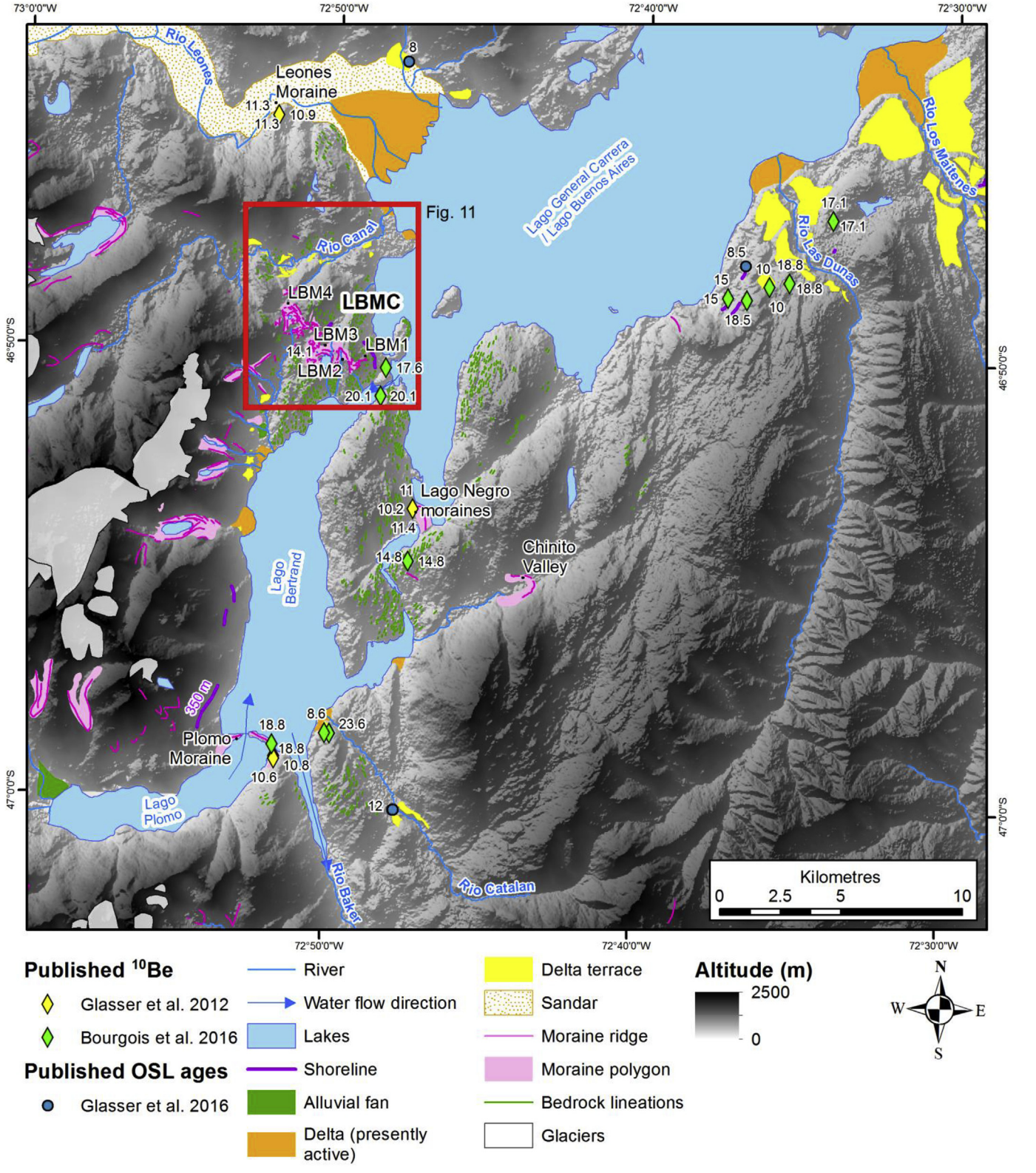

Fig. 10. Lago Bertrand and surrounding region. Field study site (Fig. 11) is indicated by red box. The Plomo, Negro and Leones moraines are highlighted. Published data includes moraines and sandar (modified from Glasser and Jansson, 2008), cosmogenic nuclide ages (diamonds) (Glasser et al., 2012; Bourgois et al., 2016) and OSL ages (blue circles) (Glasser et al., 2016). Moraines have been modified and updated. Deltas are based on original mapping and published work (Bell, 2008; Glasser and Jansson, 2008; Bell, 2009; Bourgois et al., 2016; Glasser et al., 2016; Bendle et al., 2017b; Thorndycraft et al., 2018). (For interpretation of the references to colour in this figure legend, the reader is referred to the Web version of this article.)

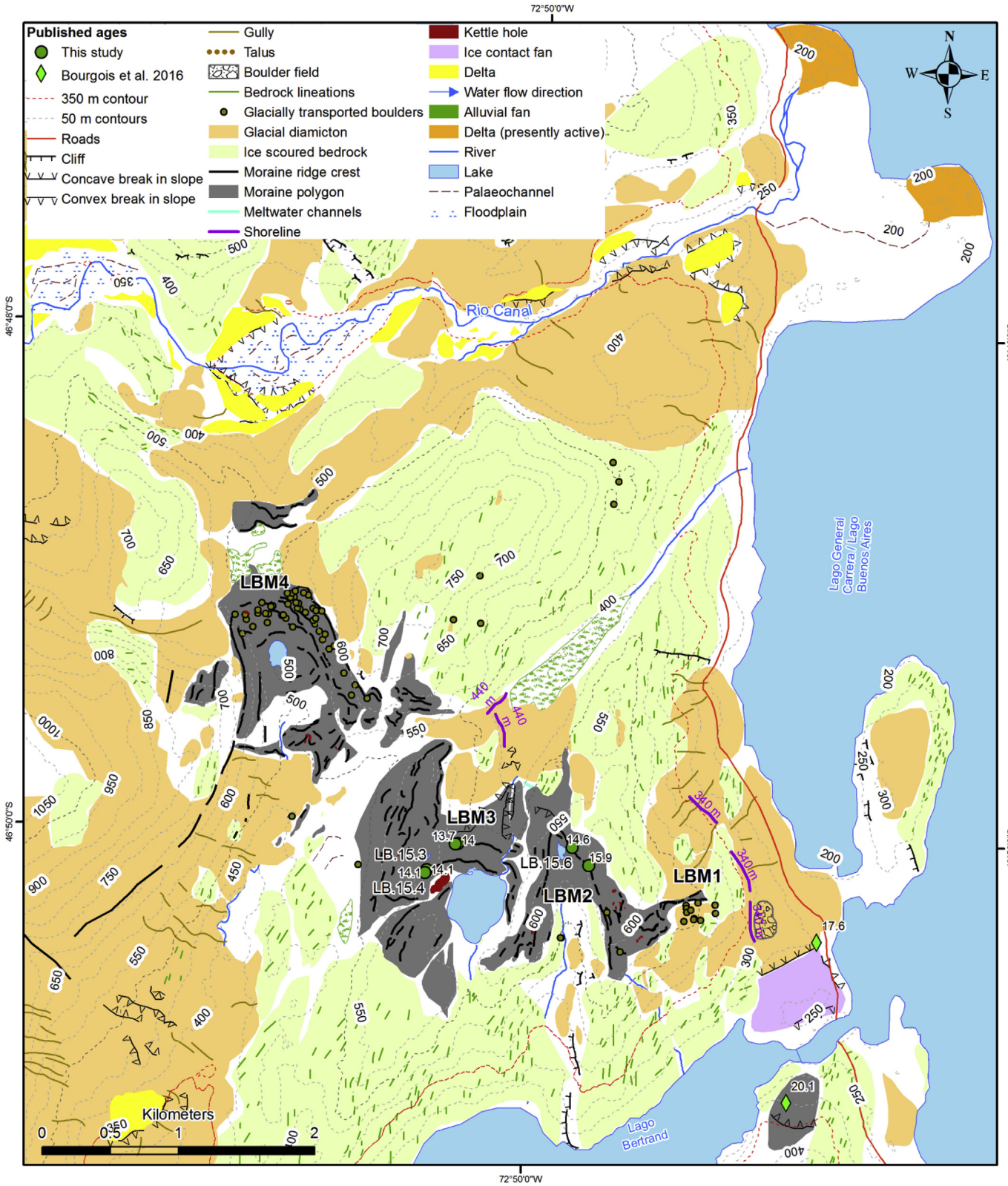

Fig. 11. Detailed geomorphological map of the LBMC, showing cosmogenic nuclide samples taken in this study with ages in ka (green circles), and published ages (diamonds). Contours derived from ASTER GDEM. (For interpretation of the references to colour in this figure legend, the reader is referred to the Web version of this article.)

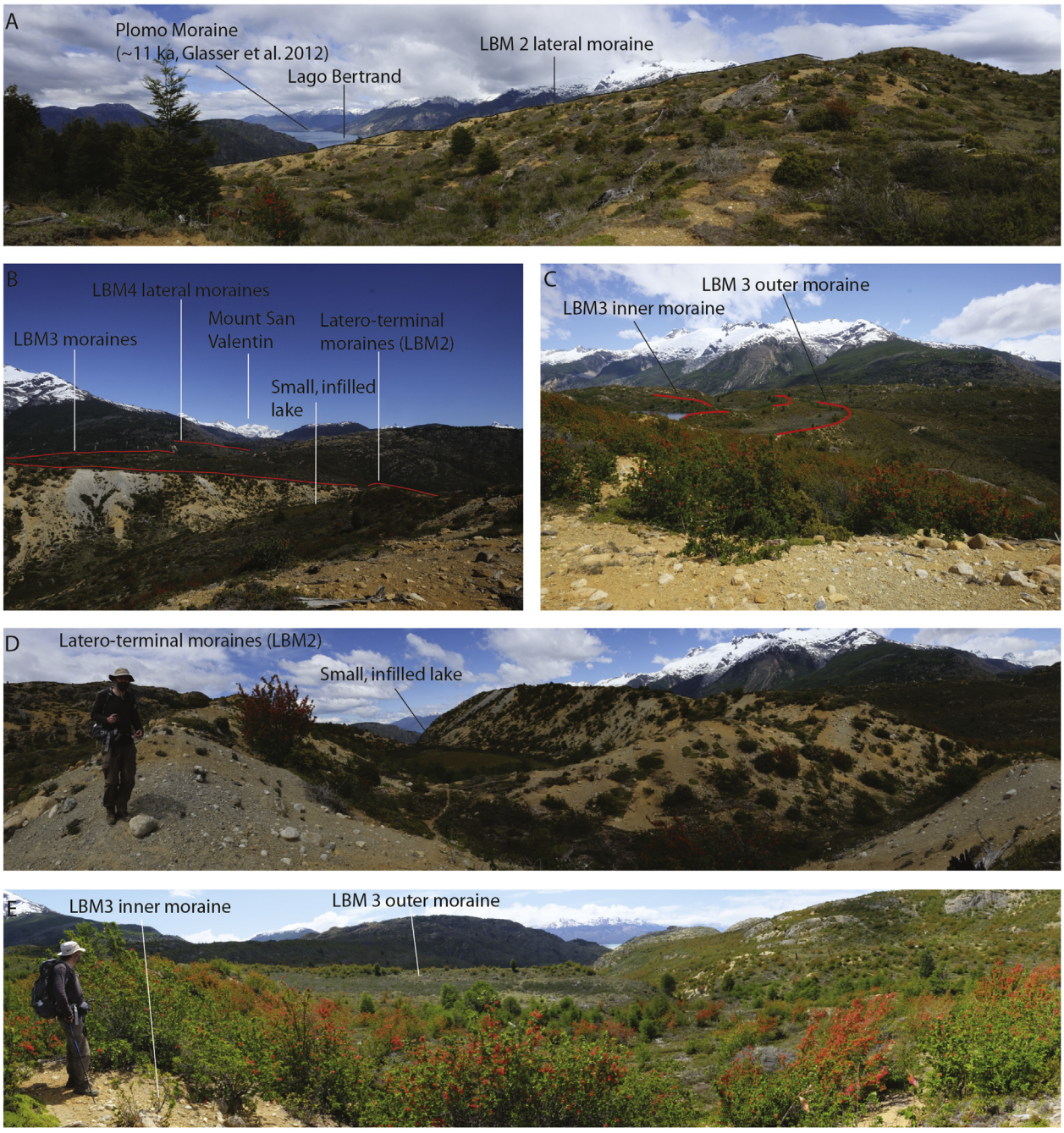

Fig. 12. Representative photographs of the Lago Bertrand moraines. LBM 2 and LBM3 are shown. Moraine ridge crests are highlighted in red. (For interpretation of the references to colour in this figure legend, the reader is referred to the Web version of this article.)

Bell, 2008; Glasser et al., 2016; Bourgois et al., 2016; Thorndycraft et al., 2018). These moraines must post-date the end of the FCMC-17 varve record (16.9 cal ka BP) to the west of Lago GCBA (Bendle et al., 2017a) and pre-date the lower-elevation Plomo moraine which formed around 11 ka (Glasser et al., 2012) (Fig. 10). Six samples were collected from the LBMC (Fig. 11) for ^{10}Be exposure-age dating; these comprise two samples from the LBM2, two samples from LBM3 inner moraine, and two samples from the LBM3 outer moraine (Table 3 and Supplementary Information). The two ages from LBM2 are 14.6 ± 0.5 and 15.9 ± 0.6 ka. The four ages from LBM3 range from 13.7 ± 0.6 to 14.1 ± 0.5 ka. The ages from the inner and outer moraines from LBM 3 are therefore within errors of each other.

The ages from the LBMC are well clustered, with LBM2 being slightly older than LBM3 (Table 3; Fig. 13). LBM2 bears two boulders with a UWM exposure age of 15.1 ± 0.7 ka. Although the oldest age boulder could be an outlier, the older age for this moraine is in agreement with the geomorphology. LBM2 is slightly higher than LBM3 and is down-ice, so this ice margin would reflect a thicker and older ice margin in the Bertrand valley.

We cannot distinguish the LBM3 inner and outer moraines, which have exposure ages within errors of each other, even though the geomorphology indicates that LBM3 is the older ice margin. The combined UWM age of these slightly lower moraines is 14.0 ± 0.6 ka. Together, the ages from LBM2 and LBM3 suggest that the glacier occupied this position in Bertrand valley from 15.1 to 14.0 ka. Since

Table 1
Sample data used to calculate cosmogenic nuclide exposure ages from the Esmeralda and Salto moraines. See text for analytical details. Uncertainty-weighted means (UWM) are rounded to nearest 100 years and presented as ka. †Recalculated ages from Glasser et al. (2012). Ages referred to in the text are highlighted.

Location	Sample ID	Latitude (dd)	Longitude (dd)	Elevation (m a.s.l)	Sample thickness (cm)	Shielding correction	Quartz mass (g)	^{10}Be (atoms/g)	Erosion rate 0 mm/kyr			Erosion rate 1 mm/kyr	
									^{10}Be LM age (yrs)	Internal uncertainty (yrs)	External uncertainty (yrs)	^{10}Be LM age (yrs)	External uncertainty (yrs)
Esmeralda latero-terminal moraine	C.15.2	-47.3195	-72.5615	512	5	0.9986	19.334	81093 ± 2780	13010	450	690	13150	700
	C.15.3	-47.3198	-72.5615	508	4	0.9986	16.564	81195 ± 2828	12970	460	690	13110	700
	C.15.8	-47.2917	-72.5651	365	5	0.9985	20.204	69717 ± 3253	12760	600	790	12900	800
	C.15.9	-47.2917	-72.5651	365	5	0.9985	21.461	72633 ± 2531	13290	470	710	13440	720
	C.15.10	-47.2918	-72.5653	368	4	0.9985	21.452	71402 ± 2384	12930	440	690	13070	690
UWM (ka)									***13.0***	***0.2***	***0.6***		
Moraine Mounds†	LE1	-47.3367	-72.5880	365	5	0.991		69800 ± 4400	12750	810	953	12890	970
	LE2	-47.3370	-72.5880	365	5	0.98		65100 ± 2700	1189	500	685	12010	700
UWM (ka)									***12.1***	***0.4***	***0.6***		
Salto Moraines (below 350 m asl shoreline)	C.15.6	-47.2946	-72.6678	338	3	0.9992	14.637	64967 ± 2385	11980	450	650	12100	660
	C.15.5	-47.2945	-72.6710	349	5	0.9992	19.834	65318 ± 2258	12120	420	641	12250	650
UWM (ka)									***12.1***	***0.3***	***0.5***		
Salto Moraines (above 350 m asl shoreline)	C.15.7	-47.2955	-72.6582	359	3	0.9957	16.201	68745 ± 2437	12478	448	667	12610	681

Table 2
Recalibrated radiocarbon ages from published data (Turner et al., 2005).

Location	Sample ID	Latitude (dd)	Longitude (dd)	Elevation (m a.s.l)	Material dated	δ^{13}C	^{14}C age	^{14}C uncertainty	2σ minimum	2σ maximum	Calibrated age (mean)	2 σ uncertainty
Salto Moraines kettle holes	AA35091	−47.2975	−72.6533	333	Peat	−31.5	13550	95	15967	16603	16285	636
	AA42408	−47.2974	−72.6531	332	Macrofossils	−32.2	13107	81	15323	15940	15631	617
	AA35092	−47.2980	−72.6557	340	Peat	−28.6	12105	80	13742	14129	13936	387
	AA42409	−47.29792	−72.6557	340	Macrofossils	−30.7	11578	71	13215	13541	13378	326

the moraines are overprinted by the 400 m shoreline, the glacier advance occurred during the existence of the 400 m Deseado lake, and then retreated, which enabled the formation of a unified palaeolake through Río Baker.

7. Discussion

7.1. Glaciolacustrine landsystem

We present a new landsystem model for the Salto Valley (Fig. 15), with valley glaciers terminating in glaciolacustrine environments forming sub-subaqueous, asymmetric morainal banks and conversely, sharp-crested and arcuate subaerial moraines (Fig. 15A). The glaciolacustrine landform assemblage includes raised deltas, palaeoshorelines at a consistent altitude, and subaqueous fans (Fig. 15B). The moraines formed before large drops in the altitude of the valley floor, indicating that calving and lake depth was one of the main controls on glacier terminus position. These glaciolacustrine landforms are associated with well-sorted laminated silts and clays, such as those deposited north of the Esmeralda moraines, and stratified diamictons and gravels in the morainal banks. The horse-shoe shaped scars on the steep ice-distal slope of the Esmeralda wedge-shaped morainal bank represent sediment gravity flows into the water. This landform assemblage, with sediments deposited subaqueously in front of the ice margin by underflows and turbidity currents, is similar to the glaciomarine landsystem modelled by Dowdeswell et al. (2015) for Chilean fjords in southern Patagonia. However, this more confined environment results in a greater diversity of landforms and sediments, and glaciolacustrine deposition is likely to be more strongly influenced by underflows into a sediment-stratified proglacial lake (cf. Ashley, 2002; Johnsen and Brennand, 2008; Sugiyama et al., 2016; Lang et al., 2017), whereas freshwater bouyant plumes are more dominant in glaciomarine settings (cf. Dowdeswell et al., 2015, 2016).

We suggest that the large asymmetric morainal banks formed during periods of glacier stabilisation, and that ice-contact fans built up along the valley sides during recession. An association of morainal banks and ice-contact/proximal fans is common in temperate glacial environments with abundant meltwater (Dowdeswell et al., 2016). They require an ice margin to be stable for some years to decades (Dowdeswell et al., 2015). Ice contact fans typically form at the outlet of structural valleys and behind grounding zone wedges (Dietrich et al., 2017), which is the case for the Juncal Fan, situated as it is behind the Esmeralda and Salto morainal banks. The ice contact fan in Lago Bertrand is likewise situated at the outlet of a structural valley.

The Juncal Fan is steeply incised by a deep channel, with an alluvial fan at its base. We interpret this as a subaerial meltwater channel that formed following the drop in lake level. To form a meltwater channel, the glacier must have been very proximal, probably just following recession from the Moraine Mounds directly across the valley mapped by Glasser et al. (2012), possibly to a pinning point at the mouth of the valley. The Juncal Fan then formed between the ice and the hillside. This meltwater channel positions the glacier margin when Lago Chalenko drained.

We surmise that care must be taken in all areas east of the NPI not to sample boulders that may have been underwater, given that ice-marginal lakes reached high elevations, e.g. up to 500 m asl in the more distal parts of the Cochrane valley (Turner et al., 2005; Hein et al., 2010), or to acknowledge that exposure ages from boulders from subaquatic moraines will date the timing of lake drainage.

7.2. Regional chronostratigraphy

Beyond our study, there are few other moraine limits dated in the LBMC region. In Figs. 13 and 14, it is clear that the samples below the 350 m Lago Chalenko level from the Chacabuco Moraines

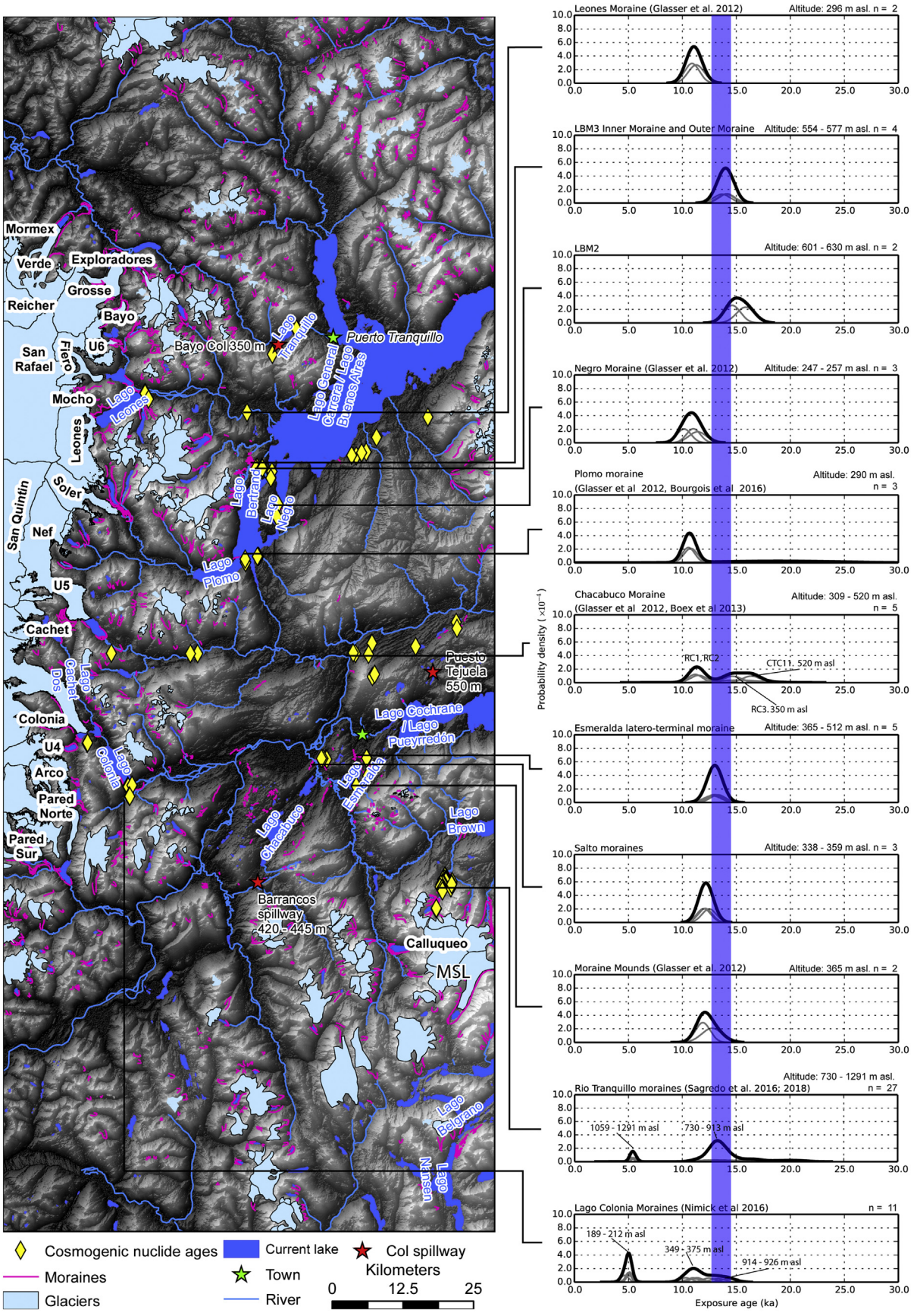

Fig. 13. Normal kernel density estimates of new and published cosmogenic nuclide ages. Each (grey) Gaussian at the bottom of the plot represents a single age, with the width corresponding to 1 σ error in the age uncertainty (internal uncertainties). Each Gaussian has the same area. High, narrow Gaussian distributions therefore have more precise age

(also known as the Río Colonia Moraine Mounds; Glasser et al., 2012), and the Leones, Plomo and Negro moraines (Fig. 10; Fig. 13; Fig. 14) are substantially younger than the higher samples from the subaerial lateral moraines above, with ages centred on 11–12 ka. We suggest that these ages constrain the timing of lake drainage (cf. Thorndycraft et al., 2018). We note that the higher sample RC3 from Glasser et al. (2012), taken at 350 m asl, yields an older recalculated age of 14.6 ± 0.8 ka, which supports this suggestion that younger, lower ages relate to the draining of Lago Chalenko (see Chacabuco Moraines in Fig. 14).

The Lago Negro Moraine is likely synchronous with the ice contact fan that links to the lateral moraines at Bertrand col. The young age of the Lago Negro Moraine therefore is likely to be associated with shielding by lake waters. The Plomo moraine records a later glacier stabilisation once drainage had opened up and the palaeolake had drained to its current level through Río Baker; this advance could be climatically driven, or related to a dynamic change in environment following lake drainage and a change in calving conditions. These younger moraine limits are also lower in altitude, and represent a progressive thinning and recession to key pinning points (Barr and Lovell, 2014).

Further indications of a readvance of the NPI during the ACR come from Lago Colonia (Nimick et al., 2016), who dated a series of moraines (samples ARCO1, 3, 4) from 12.4 to 14.2 ka. The lower-elevation CLARO moraine (samples 1, 2, 3, 5) had boulders with exposure ages ranging from 10.3 to 11.4 ka (these samples are all marginally above 350 m asl, and the context with the 350 m palaeolake Chalenko is poorly constrained). The UWM exposure age of the RT1 moraine from Tranquilo Glacier from MSL (Sagredo et al., 2018) is 13.5 ± 0.2 ka.

The ages yielded from the LBMC are older than those associated with the Colonia, Tranquilo and Calluqueo advances. The weighted means of 15.1 ± 0.7 ka to 14.0 ± 0.6 ka indicate that Soler Glacier reached these moraines during the early part of the ACR, while the Esmeralda Moraines date to the later part of the ACR. We emphasise that the presence of Soler Glacier at Bertrand col prevents the formation of the 350 m asl unified lake in the Lago CP and Baker valley, as this lake drained north through the Bayo col (near Puerto Tranquillo; see Fig. 1), so there is independent geomorphological evidence for these older ages.

7.3. Glacial evolution during the Antarctic Cold Reversal and Early Holocene

We use our new geomorphic and chronostratigraphic data alongside published moraines and ages to constrain dynamic ice behaviour and palaeolake-glacier interactions from 16 ka, through the ACR and into the Early Holocene.

7.3.1. Phase A: 16 ka – glacial recession

At 16 ka, the glaciers are well receded from their LGM positions at the far ends of Lago CP and Lago GCBA but are likely still coalesced in the eastern valleys draining the NPI. Between 17.0 and 16.0 ka, ice in the Chacabuco Valley had retreated to the Maria Elena moraines (Fig. 1) (Boex et al., 2013), with the ice-dammed Lago Chacabuco draining over Puesto Tejuela (550 m asl) into Lago CP (Glasser et al., 2016) (Fig. 16A). Glaciolacustrine influence in Lago Edita in this area had ceased by 19.4 cal ka BP, suggesting that the highest lake in Valle Chacabuco may have drained even earlier (Henríquez et al., 2017); however, we suggest instead that Lago Edita may represent a small ice-dammed lateral lake rather than the regional palaeolake, which drained later.

At this time, ice was more extensive in Valle Grande, with NPI and MSL-sourced glaciers confluent and damming the western end of Lago CP, which therefore drained to the Atlantic via a ~500 m outflow (Turner et al., 2005; Hein et al., 2010).

At 16 ka, Barrancos Glacier, Pared Norte Glacier and Colonia Glacier were confluent in Valle Grande, forming a large trunk glacier terminating in 550 m Palaeolake Chacabuco. In the Salto Valley, the 710 m Esmeralda lateral moraine may delimit the ice surface in this valley at this time. Palaeolake GCBA was at the 400 m Deseado level and drained eastwards towards the Atlantic through Río Deseado (cf. Bourgois et al., 2016).

7.3.2. Phase B: 15 ka – Soler Glacier stabilisation

Soler Glacier stabilised at Bertrand Col, therefore still blocking Lago GCBA drainage through Río Baker, resulting in separate lakes at different elevations. An arm of Soler Glacier was also present at the Negro Moraines, which formed underwater as an ice-contact fan (Thorndycraft et al., 2018), and an arcuate moraine denotes ice extent in Chinito valley (Fig. 16B). It is possible that ice stabilisation initially occurred due to a narrow bedrock pinning point (cf. Barr and Lovell, 2014) at Bertrand Col. The early ACR ages from the LBM3 moraines (14.0 ± 0.3 ka) suggest that climate cooling helped maintain Soler Glacier at this position for over a thousand years. Our new ages from the LBMC are essential for timing the damming of the Bertrand Col and the separation and unification of the Lago CP and Lago GCBA ice-dammed lakes.

There is no equivalent ice margin mapped from Barrancos Glacier or Calluqueo Glacier. The mapping of the Barrancos spillway at the head of the Juncal valley (Thorndycraft et al., 2018), with a lower 420 m col and a higher spillway at ~460 m asl, required Barrancos Glacier to recede sufficiently in the Juncal valley to allow drainage over the Barrancos col and in to the lower Baker valley. The opening of this spillway is dated by the abandonment and cessation of glaciolacustrine influences at Lago Augusta at 15.7–14.8 cal ka BP (Villa-Martínez et al., 2012; Thorndycraft et al., 2018). This is supported by independent evidence suggesting that the lake level in Lago CP dropped below ~500 m asl at 15.5 ka (Hein et al., 2010).

The northward-flowing Barrancos Glacier had an accumulation area in the Barrancos Mountains immediately south of Monte San Lorenzo. This glacier was therefore independent of the NPI. The opening of the Barrancos spillway and recession of Barrancos Glacier indicates that NPI and ice from the eastern massifs (MSL and Barrancos Mountains; Fig. 1) were separating. The early recession of Barrancos Glacier, before Calluqueo Glacier, may have been caused by its smaller accumulation area and lower altitude, rendering it sensitive and vulnerable to both climatic changes and calving-induced recession.

It is likely that Calluqueo Glacier was advanced north of the Esmeralda Moraine, calving into the 460 m palaeolake in the Lago CP valley. A lack of shorelines above 350 m asl on Cerro Ataud and geomorphic evidence from the Esmeralda Moraines suggests that the glacier was beyond the Esmeralda limits.

There are no dated ice limits of Nef Glacier at this time, however, the ~460 m asl shorelines can be traced in the Baker valley to Soler Glacier so we hypothesise that by the time the 420–460 m palaeolake formed, Nef Glacier had receded towards its valley confluence with Río Baker (Fig. 16B).

determinations. The smooth black lines are the sum of the individual Gaussians. The peak of the smooth black line highlights clusters of ages. The blue bar indicates the timing of the Antarctic Cold Reversal (ACR). Published ages from multiple sources (Glasser et al., 2012; Boex et al., 2013; Bourgois et al., 2016; Nimick et al., 2016; Sagredo et al., 2016, 2018). (For interpretation of the references to colour in this figure legend, the reader is referred to the Web version of this article.)

Table 3
Details for Lago Bertrand cosmogenic nuclide samples. See text for analytical details. Uncertainty weighted means (UWM) are rounded to nearest 100 years and presented as ka. Ages referred to in the text are highlighted (0 cm/yr erosion rate; internal uncertainties).

Location	Sample ID	Latitude (dd)	Longitude (dd)	Elevation (m asl)	Sample thickness (cm)	Shielding correction	Quartz mass (g)	^{10}Be (atom/g)	Erosion rate of 0 cm/kyr			Erosion rate of 1 mm/kyr	
									^{10}Be LM Age (yrs)	Internal uncertainty (yrs)	External uncertainty (yrs)	^{10}Be LM age (yrs)	External uncertainty (yrs)
LBM2	LB.15.6	-46.8341	-72.8292	601	1.5	0.9970	21.143	100484 ± 3423	14610	510	770	14790	790
	LB.15.7	-46.8352	-72.8276	630	4	0.9902	9.319	109008 ± 3934	15860	580	860	16070	880
UWM (ka)									***15.1***	***0.4***	***0.7***		
LBM3	LB.15.3	-46.8358	-72.8432	577	5	0.9982	22.743	92367 ± 3137	14100	490	740	14270	760
inner moraine	LB.15.4	-46.8360	-72.8433	575	4	0.9982	17.870	93179 ± 3112	14103	480	740	14300	750
LBM3	LB.15.2	-46.8340	-72.8403	554	2	0.9954	11.422	92133 ± 3340	14040	520	760	14210	780
outer moraine	LB.15.5	-46.8340	-72.8405	566	4	0.9954	10.402	89429 ± 3539	13710	550	770	13870	790
UWM (ka)									***14.0***	***0.3***	***0.6***		

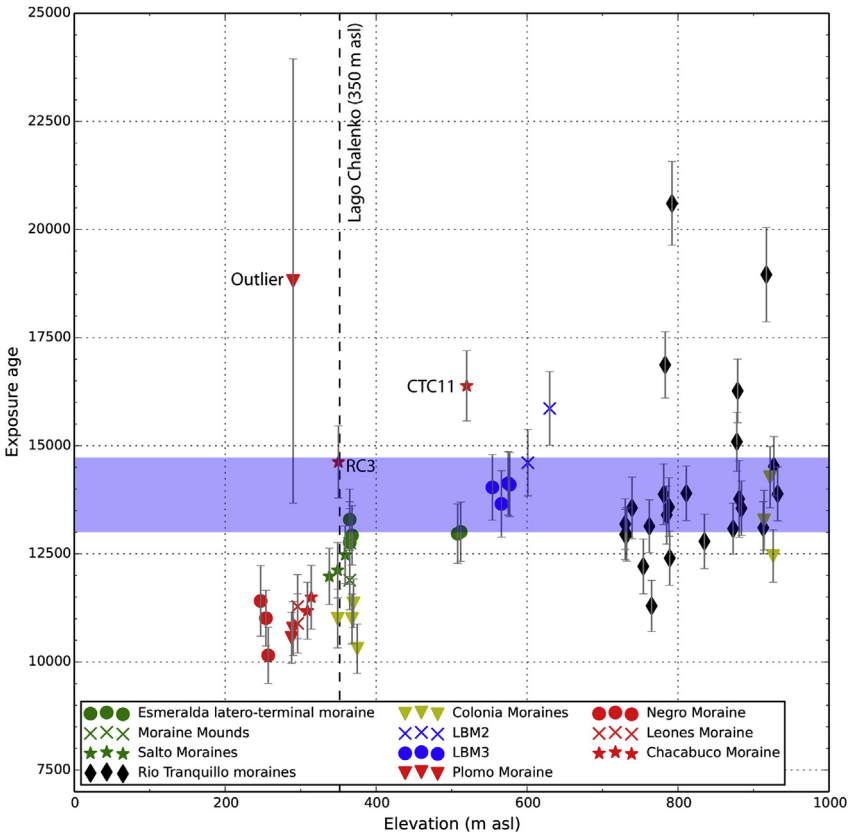

Fig. 14. Age-altitude scatter plot of our new ages and recalculated published ages (Glasser et al., 2012; Nimick et al., 2016; Bourgois et al., 2016; Sagredo et al., 2016, 2018). Blue bar indicates duration of ACR, black dashed vertical line indicates elevation of Lago Chalenko. (For interpretation of the references to colour in this figure legend, the reader is referred to the Web version of this article.)

7.3.3. Phase C: 13 ka – Calluqueo Glacier and Tranquilo Glacier advance

Calluqueo Glacier stabilised at Cerro Ataud forming the Esmeralda and Salto moraines at 13.0 ± 0.6 ka. The lake level had fallen to the ~350 m asl Lago Chalenko elevation. Soler Glacier had retreated up the Bertrand Valley allowing Lago GCBA and Lago CP to unify through the Baker valley, with drainage to the Pacific through the by the now opened Bayo col following recession of Exploradores Glacier and other northerly glaciers of the NPI from the Río Norte/Bayo valley (see Fig. 1) (Glasser et al., 2016). We argue that our multiple cosmogenic ages and the morphostratigraphic relationships we have identified between the moraines and Lago Chalenko are more reliable than the single OSL date used to infer a later opening of the Bayo valley (Glasser et al., 2016). The presence of Lago Chalenko in Valle Grande and the Cochrane basin indicates that NPI ice was still blocking Río Baker, likely in the sector from the Colonia to Los Ñadis confluences.

Tranquilo Glacier on the northern side of Monte San Lorenzo also underwent a readvance at this time (UWM age of 13.5 ± 0.2 ka and 13.0 ± 0.4 ka respectively) (Sagredo et al., 2018) (Fig. 1; Fig. 13; Fig. 14).

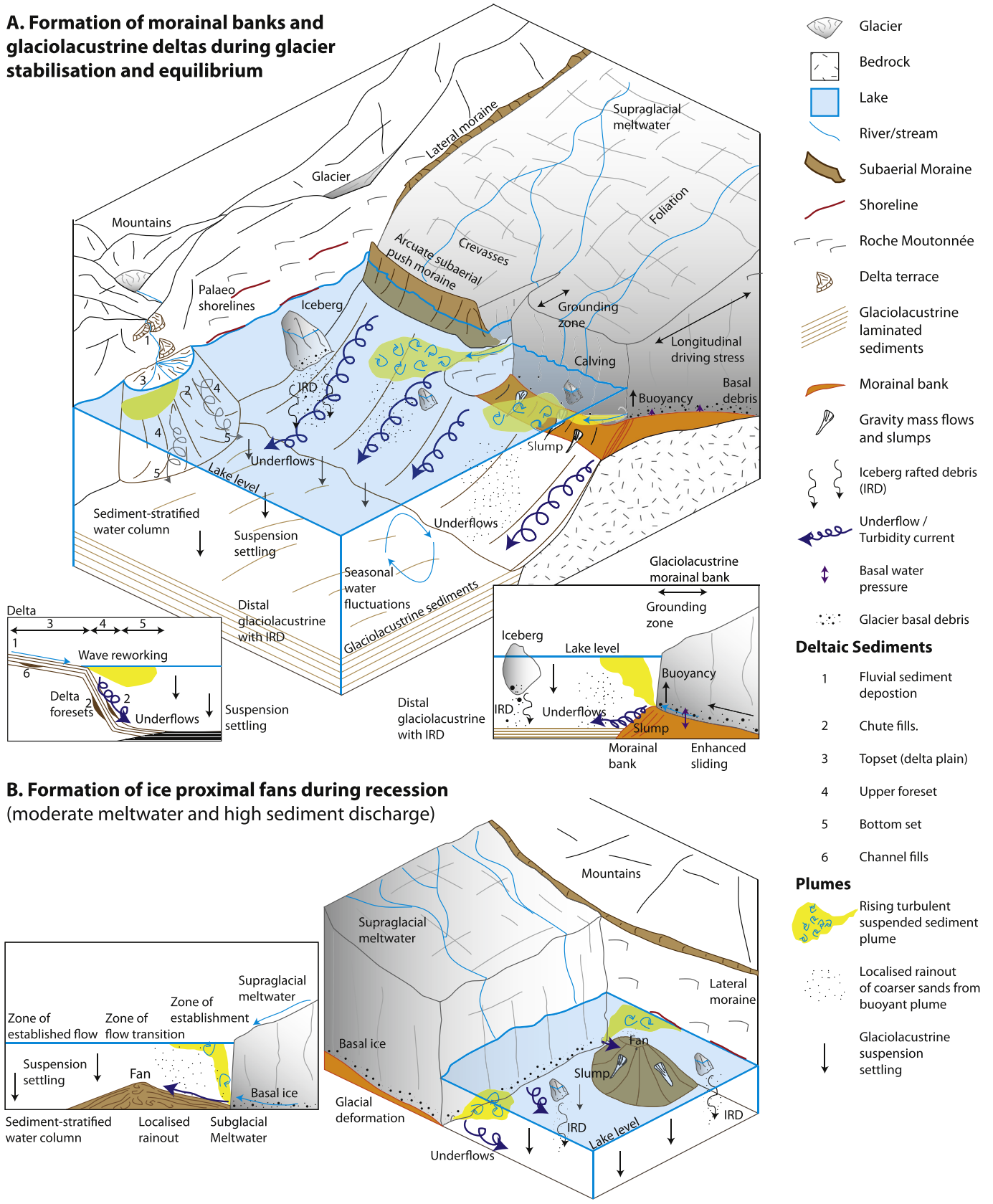

Fig. 15. A: 3D plan view and along-profile 2D views illustrating glaciolacustrine sedimentary processes. Following glacier advance and stabilisation, a large subaqueous morainal bank is built. Whilst the lake is dammed at the higher level, glaciolacustrine terraces and shorelines develop beyond the glacier limits. Modified from Powell (1990), Longhitano (2008), Dowdeswell and Vásquez (2013), Dowdeswell et al. (2015, 2016) and Carrivick and Tweed (2013). B: 3D plan view and 2D along-profile view illustrating the formation of an ice-proximal fan during glacier recession. These features typically form under moderate meltwater and a high sediment discharge scenario. Modified from Powell (1990), Lønne (1995) and Batchelor and Dowdeswell (2015).

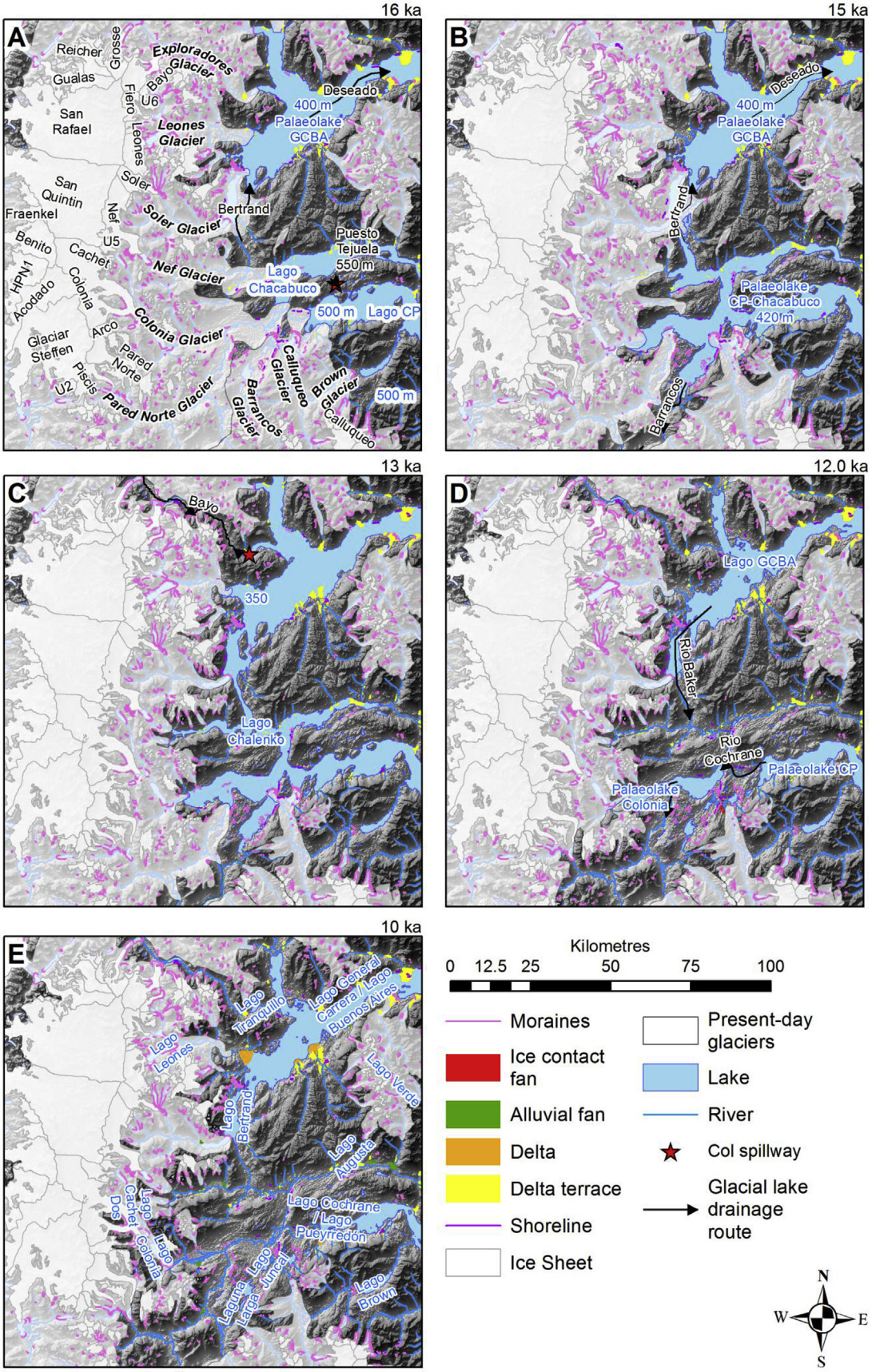

Fig. 16. Reconstruction of key stages in glacier and lake evolution for the NPI and Monte San Lorenzo. MSL = Monte San Lorenzo.

7.3.4. Phase D: 12 ka –post ACR recession, lake drainage, stabilisation during the Younger Dryas

Glacier recession resulted in the formation of the recessional Moraine Mounds (365 m asl) (Glasser et al., 2012) at 12.1 ± 0.6 ka. Lago Chalenko was still extant at this time, imprinting shorelines at 350 m asl around Cerro Ataud, Lago Esmeralda, and in the Juncal Valley (Figs. 3 and 4). On the opposite side of the Salto Valley, the Juncal Fan was forming. The Juncal Fan is dissected by a subaerial meltwater channel, suggesting the lake drained soon after the fan formed, while the ice remained in a proximal position, most likely at or near the Moraine Mounds. This fits, within the dating uncertainties, the exposure age from the subaqueous boulders from the Salto Moraines (12.1 ± 0.5 ka), and a Baysian modelled age of 12.4–11.8 ka for the timing of lake drainage (Thorndycraft et al., 2018). Pulsed drainage is suggested by the lower stepped shorelines imprinted upon the Salto Moraines (Fig. 4). The drainage of Lago Chalenko indicates that the Pared Norte Glacier had receded southwards, opening up the Río Baker drainage route to the Pacific Ocean.

7.3.5. Phase E: 10–11 ka – Early Holocene ice limits

A stabilisation of some outlet glaciers during the Younger Dryas may have occurred, with clusters of ages around 10–11 ka (e.g. see Fig. 16). Although some of these ages represent boulders sampled from under water, moraines with boulders above the surface of Lago Chalenko and well inside the ACR limits are dated to this time for Colonia Glacier (Nimick et al., 2016) and Tranquilo Glacier (Sagredo et al., 2018), as well as at the Moraine Mounds in the Salto Valley (Glasser et al., 2012). A limit congruent with the Younger Dryas but well inside the ACR limit has also been observed at the Herminita moraines in Lago Argentino (Strelin et al., 2011; Kaplan et al., 2011) and Tierra del Fuego (Menounos et al., 2013). These data suggest that although the ACR advance was much more significant, there may have been a smaller Younger Dryas readvance in Patagonia as well.

By 10 ka, the lakes and drainage routes around the NPI had reached their present-day configuration (Fig. 16E). The glaciers had receded up their valleys towards modern-day positions. Ages of 10.2 ± 0.5 to 11.1 ± 0.6 ka at elevations of 1120 m asl from a lateral moraine of Nef Glacier (Glasser et al., 2012) suggest that Nef Glacier had retreated substantially up-valley. Lateral moraines only 14 km from the ice margin around Lago Colonia (349–375 m asl) yield exposure ages of 10.1 ± 1.0 to 11.2 ± 1.1 ka (Nimick et al., 2016). Soler Glacier was at the Plomo Moraine (ages of 10.4 ± 0.5 and 10.6 ± 0.6 ka; Glasser et al., 2012).

7.4. Glacier dynamics in Patagonia during the ACR

Antarctic ice cores indicate that the ACR was a period of strong cooling (Fudge et al., 2013; Wais Divide Project Members, 2015). Numerical modelling studies have suggested that the Patagonian Ice Sheet stabilised during the ACR (14.7–13.0 ka) (Hubbard et al., 2005), which is in line with palaeoclimatic studies that suggest that the influence of the ACR extended to at least 40°S, with cooling strongest in the South Atlantic (Pedro et al., 2016). Marine sediment cores also support cooling in the South Pacific near Chile at 41°S during the ACR (Kaiser et al., 2007). This cooling resulted in advances of glaciers from the tropical Andes (Jomelli et al., 2014, 2017), NPI (this study; Turner et al., 2005), MSL (this study; Sagredo et al., 2018), and Torres del Paine (50°S) (Fogwill and Kubik, 2005; Moreno et al., 2009; García et al., 2012). Palynological data from Lado Edita, near Lago Augusta, suggest that this period of time was also associated with an increase in precipitation (Henríquez et al., 2017), which, in combination with lower temperatures associated with the ACR, would have encouraged glacier advance. However, although there is emerging evidence of wide-spread glacier advances during the ACR in Patagonia, the exact timing of the moraine formation is spatially variable, even in the same region. Our data show that topographic constraints, pinning points and calving dynamics in ice-dammed lakes exerted a significant control on the glaciers.

The exposure ages from the LBMC latero-terminal moraines and associated ice-contact fan, which lie beyond the limits of the Plomo and Negro moraines, suggest that Soler Glacier stabilised at the Lago Bertrand col during the early part of the ACR (Jouzel et al., 2001; Morgan, 2009; Putnam et al., 2010; Pedro et al., 2016). Soler Glacier occupied the LBMC from 15.1 ± 0.7 to 14.0 ± 0.6 ka, when it was calving into the 400 m Deseado level palaeolake. Topographical constraints encouraged ice-margin stabilisation and moraine formation (Barr and Lovell, 2014) against a background of a cooling climate.

The Esmeralda Moraine was formed subaerially at 13.0 ± 0.6 ka, at which time there was a unified 350 m Lago Chalenko in both the Lago CP and Lago GCBA valleys. Our geomorphological mapping independently demonstrates that the moraines cannot have formed synchronously, because Soler Glacier at the Bertrand Moraines blocks the formation of the unified 350 m Lago Chalenko. Lago Chalenko likely had a significant influence on the ice-margin stabilisation, with ice margins forming at topographic highs at the Esmeralda and Salto margins. Deep water beyond these moraines encouraged calving and limited the size and extent of the glacier.

Glaciers on the northern flank of MSL underwent smaller advances at 13.5 ± 0.2 ka (Sagredo et al., 2018), highlighting the important role of glacier catchment and aspect on driving glacier advances. Sagredo et al. (2018) reconstruct a glacier occupying the RT1 moraines in Río Tranquilo Valley with a length of ~14 km and an ELA 260 ± 20 m below modern values (1815 ± 10 m) (Falaschi et al., 2013; Sagredo et al., 2018). We do not calculate ELAs at this time for Calluqueo Glacier, as it and Soler Glacier are calving into deep water, which affects mass balance (cf. Rea, 2009). However, Calluqueo Glacier was clearly much more extensive than Tranquilo Glacier during the ACR. This differential could reflect changes in the ice divide location, and the additional accumulation area afforded to Calluqueo Glacier by the Barrancos Mountains (Fig. 16C). Today, glaciers in Río Tranquilo valley are less extensive than Calluqueo Glacier (50.9 km^2; 2013; Falaschi et al., 2016), which has a much larger accumulation area (Fig. 2). Glaciers on the western flank of Monte San Lorenzo also have present-day ELAs that are 1700–1750 m asl, whilst the eastern, drier sectors have higher ELAs >1800 m asl (Falaschi et al., 2013). Depressed ELAs on the western portion of MSL could contribute to a larger readvance in the Salto Valley. However, the interpretation by Sagredo et al. (2018) is consistent with our argument that a large readvance occurred during the ACR in MSL. We also note that Barrancos Glacier receded before Soler Glacier and Calluqueo Glacier, likely due to its smaller catchment in the Barrancos Mountains (cf. Fig. 2) combined with a lake-terminating margin. By the time of the Younger Dryas, the glaciers had all substantially retreated from their ACR positions, but there was a stabilisation of the glaciers leading to moraine formation at this time; exposure ages from Colonia Glacier moraines show that glaciers were not far beyond their Little Ice Age Limits by ~12.1 ka (Nimick et al., 2016). These data highlight the importance of not assuming that similar-sized moraines in adjacent valleys necessarily relate to synchronous advances. A detailed landsystems approach is recommended as a methodology to understand the context of moraine formation, and to infer past glacial dynamics from moraine age.

8. Conclusions

In this study, we used geomorphological mapping and cosmogenic nuclide dating from outlet glaciers of the eastern Northern

Patagonian Icefield and the Monte San Lorenzo ice cap in central Patagonia, South America, to provide new, detailed, process-based interpretations for landform formation in a glaciolacustrine landsystem. We highlight for the first time the detailed mechanisms by which subaqueous morainal banks formed during the deglaciation of central Patagonia, and we constrain the timing of ice-lake interactions. We argue that recognition of subaqueous landforms and environments is critical to developing a strategy for dating past glacial fluctuations.

Our cosmogenic exposure-age data demonstrate that the largest readvance since the LGM in central Patagonia occurred during the ACR, with further glacier recession and lake drainage (12.0 ± 0.6 ka) occurring rapidly during warming after the ACR. Our data show that whilst this readvance was broadly climatically driven, the timing of individual outlet glacier advances was asynchronous and spatially variable, subject to external controls such as proglacial lakes and calving, aspect and accumulation area size, and bedrock pinning points.

We mapped and dated moraines from above known palaeolake levels of Lago GCBA, identifying an advance of Soler Glacier to the col between Lago Bertrand and Lago GCBA, where it formed a subaqueous ice-contact fan as it calved into a 400 m high palaeolake. Cosmogenic nuclide ages from these moraines yielded uncertainty-weighted mean ages of 15.1 ± 0.7 ka for the oldest, highest moraines, and 14.0 ± 0.6 ka for the inner moraines, indicating that the glacier was likely in this position for some 1000 years. The highest and oldest moraine ages pre-date the ACR indicating that the local topography with a narrow valley exiting into the western embayment of Lago GCBA encouraged topographic pinning here (cf. Barr and Lovell, 2014).

By contrast, we date the most distal ice margin of Calluqueo Glacier, terminating at the Esmeralda push moraine, to towards the end of the ACR at 13.0 ± 0.6 ka. The ice margin here was contemporaneous with Lago Chalenko (350 m asl). Subaqueous morainal banks delimit the ice margin, with a glaciolacustrine landsystem that includes ice-scoured bedrock, glacial diamicton plastered onto valley sides, perched delta terraces, kame terraces, ice-contact fans, palaeoshorelines etched into glacigenic sediments and subaerial push and lateral moraines.

Our data demonstrates that cosmogenic nuclide exposure-age dating can be applied to constrain lake level falls where ice-lake interactions are well understood. Sampled boulders from Salto moraine, from below the Lago Chalenko lake level, were dated to 12.0 ± 0.6 ka, closely matching the age of recessional moraines at the mouth of the Salto valley (Glasser et al., 2012) and providing independent support for a Bayesian modelled age of 12.4–11.8 ka for lake drainage (cf. Thorndycraft et al., 2018). Our study adds to the growing body of evidence that there was a strong ACR signal controlling glacier fluctuations in central Patagonia, but with the caveat that this was modulated and contolled by spatially variable topographic and glaciolacustrine controls on glacier extent.

Acknowledgements

Davies and Thorndycraft undertook geomorphological fieldwork and collected cosmogenic nuclide samples in November/December 2015. Geomorphological mapping was also conducted by Davies, Thorndycraft and Martin in November/December 2016 and 2017. Fabel undertook analysis of cosmogenic nuclide samples. Fieldwork was funded by the Royal Holloway University of London Research Strategy Fund (RHUL-RSF) and NERC DTP PhD award NE/L002485/1 awarded to Martin. We thank the RHUL-RSF, Quaternary Research Association, British Society for Geomorphology, and the Geologists' Association for each part-funding analytical costs of cosmogenic nuclide analysis. We thank Maria Miguens-Rodriguez (SUERC Cosmogenic Isotope Laboratory) for the preparation of the cosmogenic nuclide samples, and staff at the SUERC AMS Laboratory, East Kilbride, are thanked for ^{10}Be measurements. We thank all landowners for allowing access to their property during fieldwork. ASTER GDEM is a product of NASA and METI. Landsat-8 images used in mapping are provided courtesy of the U.S. Geological Survey. BD and VT were supported in the field at the Bertrand moraines by Esteban, the local shepherd. All supporting data for this publication are included either in the paper or in the Supplementary Information. We thank two anonymous reviewers whose comments helped improve and clarify the manuscript.

Appendix A. Supplementary data

Supplementary data to this article can be found online at https://doi.org/10.1016/j.quascirev.2018.09.025.

References

Ackert, R.P., Becker, R.A., Singer, B.S., Kurz, M.D., Caffee, M.W., Mickelson, D.M., 2008. Patagonian glacier response during the late glacial–holocene transition. Science 321, 392–395.
Ashley, G.M., 2002. Chapter 11-Glaciolacustrine environments. In: Menzies, J. (Ed.), Modern and Past Glacial Environments. Butterworth-Heinemann, Oxford, pp. 335–359.
ASTER GDEM Validation Team, METI/ERSDAC, NASA/LPDAAC, USGS/EROS, 2009. ASTER Global DEM Validation Summary Report, p. 28.
Balco, G., 2009. MATLAB code for camel diagrams. https://cosmognosis.wordpress.com/2009/07/13/matlab-code-for-camel-diagrams/.
Balco, G., 2011. Contributions and unrealized potential contributions of cosmogenic-nuclide exposure dating to glacier chronology, 1990 - 2010. Quat. Sci. Rev. 30, 3–27.
Balco, G., 2014. Simple computer code for estimating cosmic-ray shielding by oddly shaped objects. Quat. Geochronol. 22, 175–182.
Balco, G., Stone, J.O., Lifton, N.A., Dunai, T.J., 2008. A complete and easily accessible means of calculating surface exposure ages or erosion rates from ^{10}Be and ^{26}Al measurements. Quat. Geochronol. 3, 174–195.
Barr, I.D., Lovell, H., 2014. A review of topographic controls on moraine distribution. Geomorphology 226, 44–64.
Batchelor, C., Dowdeswell, J., 2015. Ice-sheet grounding-zone wedges (GZWs) on high-latitude continental margins. Mar. Geol. 363, 65–92.
Bell, C., 2008. Punctuated drainage of an ice-dammed Quaternary lake in southern South America. Geogr. Ann. Phys. Geogr. 90, 1–17.
Bell, C.M., 2009. Quaternary lacustrine braid deltas on Lake General Carrera in southern Chile. Andean Geol. 36, 51–65.
Bendle, J.M., Palmer, A.P., Thorndycraft, V.R., Matthews, I.P., 2017a. High-resolution chronology for deglaciation of the Patagonian Ice Sheet at Lago Buenos Aires (46.5°S) revealed through varve chronology and Bayesian age modelling. Quat. Sci. Rev. 177, 314–339.
Bendle, J.M., Thorndycraft, V.R., Palmer, A.P., 2017b. The glacial geomorphology of the Lago Buenos Aires and Lago Pueyrredón ice lobes of central Patagonia. J. Maps 13, 654–673.
Bennett, M.R., 2001. The morphology, structural evolution and significance of push moraines. Earth Sci. Rev. 53, 197–236.
Bennett, M.R., Huddart, D., McCormick, T., 2000. An integrated approach to the study of glaciolacustrine landforms and sediments: a case study from Hagavatn, Iceland. Quat. Sci. Rev. 19, 633–665.
Bentley, M.J., Sugden, D.E., Hulton, N.R.J., McCullough, R.D., 2005. The landforms and pattern of deglaciation in the Strait of Magellan and Bahìa Inùtil, southernmost South America. Geogr. Ann. 87A, 313–333.
Boex, J., Fogwill, C., Harrison, S., Glasser, N.F., Hein, A., Schnabel, C., Xu, S., 2013. Rapid thinning of the Late Pleistocene Patagonian Ice Sheet followed migration of the Southern Westerlies. Sci. Rep. 3, 1–6.
Boston, C.M., Lukas, S., 2017. Evidence for restricted Loch Lomond Stadial plateau ice in Glen Turret and implications for the age of the Turret Fan. Proc. Geologists' Assoc. 128, 42–53.
Bourgois, J., Cisternas, M.E., Braucher, R., Bourlès, D., Frutos, J., 2016. Geomorphic records along the general Carrera (Chile)–Buenos Aires (Argentina) glacial lake (46°–48° S), climate inferences, and glacial rebound for the past 7–9 ka. J. Geol. 124, 27–53.
Briner, J.P., Kaufman, D.S., Manley, W.F., Finkel, R.C., Caffee, M.W., 2005. Cosmogenic exposure dating of late Pleistocene moraine stabilization in Alaska. Geol. Soc. Am. Bull. 117, 1108–1120.
Caldenius, C.C., 1932. Las glaciaciones cuaternarias en la Patagonia y Tierra del Fuego. Geogr. Ann. 14, 1–164.
Carrivick, J.L., Tweed, F.S., 2013. Proglacial lakes: character, behaviour and geological

importance. Quat. Sci. Rev. 78, 34–52.
Child, D., Elliott, G., Mifsud, C., Smith, A., Fink, D., 2000. Sample processing for earth science studies at ANTARES. Nucl. Instrum. Methods Phys. Res. Sect. B Beam Interact. Mater. Atoms 172, 856–860.
Cockburn, H.A.P., Summerfield, M.A., 2004. Geomorphological applications of cosmogenic isotope analysis. Prog. Phys. Geogr. 28, 1–42.
Coronato, A., Rabassa, J., 2011. Chapter 51 - Pleistocene Glaciations in Southern Patagonia and Tierra del Fuego. In: Jürgen Ehlers, P.L.G., Philip, D.H. (Eds.), Developments in Quaternary Sciences. Elsevier, pp. 715–727.
Cuffey, K.M., Paterson, W.S.B., 2010. The Physics of Glaciers, fourth ed. Academic Press.
Darvill, C.M., 2013. Cosmogenic nuclide analysis. In: Clarke, L., Nield, J. (Eds.), Geomorphological Techniques. British Society for Geomorphology, London.
Darvill, C.M., Bentley, M.J., Stokes, C.R., Shulmeister, J., 2016. The timing and cause of glacial advances in the southern mid-latitudes during the last glacial cycle based on a synthesis of exposure ages from Patagonia and New Zealand. Quat. Sci. Rev. 149, 200–214.
Davies, B.J., Glasser, N.F., 2012. Accelerating recession in Patagonian glaciers from the "Little Ice Age" (c. AD 1870) to 2011. J. Glaciol. 58, 1063–1084.
Dietrich, P., Ghienne, J.-F., Normandeau, A., Lajeunesse, P., 2017. Reconstructing ice-margin retreat using delta morphostratigraphy. Sci. Rep. 7, 16936.
Douglass, D., Singer, B., Kaplan, M., Mickelson, D., Caffee, M., 2006. Cosmogenic nuclide surface exposure dating of boulders on last-glacial and late-glacial moraines, Lago Buenos Aires, Argentina: interpretive strategies and paleo-climate implications. Quat. Geochronol. 1, 43–58.
Douglass, D.C., Singer, B.S., Kaplan, M.R., Ackert, R.P., Mickelson, D.M., Caffee, M.W., 2005. Evidence of early Holocene glacial advances in southern South America from cosmogenic surface-exposure dating. Geology 33, 237–240.
Dowdeswell, J.A., Canals, M., Jakobsson, M., Todd, B.J., Dowdeswell, E.K., Hogan, K.A., 2016. The variety and distribution of submarine glacial landforms and implications for ice-sheet reconstruction. Geol. Soc. Lond. Memoirs 46, 519–552.
Dowdeswell, J.A., Hogan, K.A., Arnold, N.S., Mugford, R.I., Wells, M., Hirst, J.P.P., Decalf, C., 2015. Sediment-rich meltwater plumes and ice-proximal fans at the margins of modern and ancient tidewater glaciers: observations and modelling. Sedimentology 62, 1665–1692.
Dowdeswell, J.A., Vásquez, M., 2013. Submarine landforms in the fjords of southern Chile: implications for glacimarine processes and sedimentation in a mild glacier-influenced environment. Quat. Sci. Rev. 64, 1–19.
Evans, D.J.A., 2003. Ice-marginal terrestrial landsystems: active temperate glacier margins. In: Evans, D.J.A. (Ed.), Glacial Landsystems. Arnold, London, pp. 12–43.
Evans, D.J.A., 2005. Glacial Landsystems. Hodder, London.
Evans, D.J.A., Benn, D.I., 2004. Facies description and the logging of sedimentary exposures. In: Evans, D.J.A., Benn, D.I. (Eds.), A Practical Guide to the Study of Glacial Sediments. Arnold, London, pp. 11–50.
Evans, D.J.A., Phillips, E.R., Hiemstra, J.F., Auton, C.A., 2006. Subglacial till: formation, sedimentary characteristics and classification. Earth Sci. Rev. 78, 115–176.
Fabel, D., Small, D., Miguens-Rodriguez, M., Freeman, S.P.H.T., 2010. Cosmogenic nuclide exposure ages from the 'Parallel Roads' of Glen Roy, Scotland. J. Quat. Sci. 25, 597–603.
Falaschi, D., Bolch, T., Rastner, P., Lenzano, M.G., Lenzano, L., Lo Vecchio, A., Moragues, S., 2016. Mass changes of alpine glaciers at the eastern margin of the Northern and Southern Patagonian Icefields between 2000 and 2012. J. Glaciol. 63, 258–272.
Falaschi, D., Bravo, C., Masiokas, M., Villalba, R., Rivera, A., 2013. First glacier inventory and recent changes in glacier area in the Monte san Lorenzo region (47°S), southern Patagonian Andes, south America. Arctic Antarct. Alpine Res. 45, 19–28.
Fogwill, C.J., Kubik, P.W., 2005. A Glacial Stage Spanning the Antarctic Cold Reversal in Torres del Paine (51°S), Chile, based on preliminary cosmogenic exposure ages. Geogr. Ann. Phys. Geogr. 87, 403–408.
Fudge, T., Steig, E.J., Markle, B.R., Schoenemann, S.W., Ding, Q., Taylor, K.C., McConnell, J.R., Brook, E.J., Sowers, T., White, J.W., 2013. Onset of deglacial warming in West Antarctica driven by local orbital forcing. Nature 500, 440.
García, J.-L., Hall, B.L., Kaplan, M.R., Vega, R.M., Strelin, J.A., 2014. Glacial geomorphology of the Torres del Paine region (southern Patagonia): implications for glaciation, deglaciation and paleolake history. Geomorphology 204, 599–616.
García, J.L., Kaplan, M.R., Hall, B.L., Schaefer, J.M., Vega, R.M., Schwartz, R., Finkel, R., 2012. Glacier expansion in southern Patagonia throughout the Antarctic Cold Reversal. Geology 40, 859–862.
Glasser, N., Jansson, K., 2008. The glacial map of southern South America. J. Maps 4, 175–196.
Glasser, N.F., Harrison, S., Jansson, K.N., 2009. Topographic controls on glacier sediment-landform associations around the temperate North Patagonian Icefield. Quat. Sci. Rev. 28, 2817–2832.
Glasser, N.F., Harrison, S., Schnabel, C., Fabel, D., Jansson, K.N., 2012. Younger Dryas and early Holocene age glacier advances in Patagonia. Quat. Sci. Rev. 58, 7–17.
Glasser, N.F., Jansson, K.N., Duller, G.A.T., Singarayer, J., Holloway, M., Harrison, S., 2016. Glacial lake drainage in Patagonia (13-8 kyr) and response of the adjacent Pacific Ocean. Sci. Rep. 6, 21064.
Glen, J., 1954. The stability of ice-dammed lakes and other water-filled holes in glaciers. J. Glaciol. 2, 316–318.
Gosse, J.C., Phillips, F.M., 2001. Terrestrial in situ cosmogenic nuclides: theory and application. Quat. Sci. Rev. 20, 1475–1560.
Hajdas, I., Bonani, G., Moreno, P.I., Ariztegui, D., 2003. Precise radiocarbon dating of Late-Glacial cooling in mid-latitude South America. Quat. Res. 59, 70–78.
Hein, A.S., Hulton, N.R., Dunai, T.J., Sugden, D.E., Kaplan, M.R., Xu, S., 2010. The chronology of the last glacial maximum and deglacial events in central Argentine Patagonia. Quat. Sci. Rev. 29, 1212–1227.
Henríquez, W.I., Villa-Martínez, R., Vilanova, I., De Pol-Holz, R., Moreno, P.I., 2017. The Last Glacial Termination on the eastern flank of the central Patagonian Andes (47 ° S). Clim. Past 13, 879–895.
Heyman, J., Applegate, P.J., Blomdin, R., Gribenski, N., Harbor, J.M., Stroeven, A.P., 2016. Boulder height – exposure age relationships from a global glacial ^{10}Be compilation. Quat. Geochronol. 34, 1–11.
Hogg, A.G., Hua, Q., Blackwell, P.G., Niu, M., Buck, C.E., Guilderson, T.P., Heaton, T.J., Palmer, J.G., Reimer, P.J., Reimer, R.W., Turney, C.S.M., Zimmerman, S.R.H., 2013. SHCal13 Southern Hemisphere calibration, 0–50,000 Years cal BP. Radiocarbon 55, 1889–1903.
Hubbard, A., Hein, A.S., Kaplan, M.R., Hulton, N.R.J., Glasser, N., 2005. A modelling reconstruction of the Last Glacial Maximum ice sheet and its deglaciation in the vicinity of the Northern Patagonian Icefield, South America. Geogr. Ann. 87, 375–391.
Johnsen, T.F., Brennand, T.A., 2008. The environment in and around ice-dammed lakes in the moderately high relief setting of the southern Canadian Cordillera. Boreas 35, 106–125.
Jomelli, V., Favier, V., Vuille, M., Braucher, R., Martin, L., Blard, P.-H., Colose, C., Brunstein, D., He, F., Khodri, M., 2014. A major advance of tropical Andean glaciers during the Antarctic Cold Reversal. Nature 513, 224–228.
Jomelli, V., Martin, L., Blard, P., Favier, V., Vuillé, M., Ceballos, J., 2017. Revisiting the Andean tropical glacier behavior during the Antarctic Cold Reversal. Cuadernos de Investigación Geográfica 43, 629–648.
Jouzel, J., Masson, V., Cattani, O., Falourd, S., Stievenard, M., Stenni, B., Longinelli, A., Johnsen, S.J., Steffenssen, J., Petit, J.-R., 2001. A new 27 ky high resolution East Antarctic climate record. Geophys. Res. Lett. 28, 3199–3202.
Kaiser, J., Lamy, F., Arz, H.W., Hebbeln, D., 2007. Dynamics of the millennial-scale sea surface temperature and Patagonian Ice Sheet fluctuations in southern Chile during the last 70 kyr (ODP Site 1233). Quat. Int. 161, 77–89.
Kaplan, M.R., Strelin, J.A., Schaefer, J.M., Denton, G.H., Finkel, R.C., Schwartz, R., Putnam, A.E., Vandergoes, M.J., Goehring, B.M., Travis, S.G., 2011. In-situ cosmogenic ^{10}Be production rate at Lago Argentino, Patagonia: implications for Late-Glacial climate chronology. Earth Planet Sci. Lett. 309, 21–32.
Kohl, C., Nishiizumi, K., 1992. Chemical isolation of quartz for measurement of in-situ-produced cosmogenic nuclides. Geochem. Cosmochim. Acta 56, 3583–3587.
Lal, D., 1991. Cosmic ray labeling of erosion surfaces: in situ nuclide production rates and erosion models. Earth Planet Sci. Lett. 104, 424–439.
Lang, J., Sievers, J., Loewer, M., Igel, J., Winsemann, J., 2017. 3D architecture of cyclic-step and antidune deposits in glacigenic subaqueous fan and delta settings: Integrating outcrop and ground-penetrating radar data. Sediment. Geol. 362, 83–100.
Lang, J., Winsemann, J., 2013. Lateral and vertical facies relationships of bedforms deposited by aggrading supercritical flows: From cyclic steps to humpback dunes. Sediment. Geol. 296, 36–54.
Longhitano, S.G., 2008. Sedimentary facies and sequence stratigraphy of coarse-grained Gilbert-type deltas within the Pliocene thrust-top Potenza Basin (southern Apennines, Italy). Sediment. Geol. 210, 87–110.
Lønne, I., 1995. Sedimentary facies and depositional architecture of ice-contact glaciomarine systems. Sediment. Geol. 98, 13–43.
Lowe, J.J., Rasmussen, S.O., Björck, S., Hoek, W.Z., Steffensen, J.P., Walker, M.J.C., Yu, Z.C., 2008. Synchronisation of palaeoenvironmental events in the North Atlantic region during the Last Termination: a revised protocol recommended by the INTIMATE group. Quat. Sci. Rev. 27, 6–17.
Lynch-Stieglitz, J., Schmidt, M.W., Curry, W.B., 2011. Evidence from the Florida straits for Younger Dryas ocean circulation changes. Paleoceanography 26. PA1205.
Martinod, J., Regard, V., Riquelme, R., Aguilar, G., Guillaume, B., Carretier, S., Cortés-Aranda, J., Leanni, L., Hérail, G., 2016. Pleistocene uplift, climate and morphological segmentation of the Northern Chile coasts (24 S–32 S): insights from cosmogenic ^{10}Be dating of paleoshorelines. Geomorphology 274, 78–91.
Massaferro, J., Larocque-Tobler, I., Brooks, S.J., Vandergoes, M., Dieffenbacher-Krall, A., Moreno, P., 2014. Quantifying climate change in Huelmo mire (Chile, Northwestern Patagonia) during the Last Glacial Termination using a newly developed chironomid-based temperature model. Palaeogeogr. Palaeoclimatol. Palaeoecol. 399, 214–224.
Mendelova, M., Hein, A., McCulloch, R., Davies, B.J., 2017. The Last Glacial Maximum and deglaciation in central Patagonia, 44° S–49° S. Cuadernos de Investigación Geográfica.
Menounos, B., Clague, J.J., Osborn, G., Davis, P.T., Ponce, F., Goehring, B., Maurer, M., Rabassa, J., Coronato, A., Marr, R., 2013. Latest Pleistocene and Holocene glacier fluctuations in southernmost Tierra del Fuego, Argentina. Quat. Sci. Rev. 77, 70–79.
Mercer, J.H., 1970. Variations of some Patagonian glaciers since the Late-Glacial; II. Am. J. Sci. 269, 1–25.
Mercer, J.H., 1976. Glacial history of southernmost South America. Quat. Res. 6, 125–166.
Moreno, P.I., Kaplan, M.R., François, J.P., Villa-Martínez, R., Moy, C.M., Stern, C.R., Kubik, P.W., 2009. Renewed glacial activity during the Antarctic Cold Reversal and persistence of cold conditions until 11.5 ka in southwestern Patagonia. Geology 37, 375–378.

Moreno, P.I., Videla, J., 2016. Centennial and millennial-scale hydroclimate changes in northwestern Patagonia since 16,000 yr BP. Quat. Sci. Rev. 149, 326–337.
Morgan, V.I., 2009. Antarctic Cold Reversal. In: Gornitz, V. (Ed.), Encyclopedia of Paleoclimatology and Ancient Environments. Springer Netherlands, Dordrecht, pp. 22–24.
Nimick, D.A., McGrath, D., Mahan, S.A., Friesen, B.A., Leidich, J., 2016. Latest Pleistocene and Holocene glacial events in the Colonia valley, Northern Patagonia Icefield, southern Chile. J. Quat. Sci. 31, 551–564.
Nishiizumi, K., Imamura, M., Caffee, M.W., Southon, J.R., Finkel, R.C., McAninch, J., 2007. Absolute calibration of ^{10}Be AMS standards. Nucl. Instrum. Methods Phys. Res. Sect. B Beam Interact. Mater. Atoms 258, 403–413.
Otto, J.-C., Smith, M.J., 2013. Geomorphological mapping. Geomorphol. Tech.
Pedro, J.B., Bostock, H.C., Bitz, C.M., He, F., Vandergoes, M.J., Steig, E.J., Chase, B.M., Krause, C.E., Rasmussen, S.O., Markle, B.R., 2016. The spatial extent and dynamics of the Antarctic Cold Reversal. Nat. Geosci. 9, 51.
Pedro, J.B., Jochum, M., Buizert, C., He, F., Barker, S., Rasmussen, S.O., 2018. Beyond the bipolar seesaw: toward a process understanding of interhemispheric coupling. Quat. Sci. Rev. 192, 27–46.
Powell, R.D., 1990. Glacimarine processes at grounding-line fans and their growth to ice-contact deltas. Geological Soc. Lond. Special Pub. 53, 53–73.
Putkonen, J., Swanson, T., 2003. Accuracy of cosmogenic ages for moraines. Quat. Res. 59, 255–261.
Putnam, A.E., Denton, G.H., Schaefer, J.M., Barrell, D.J.A., Andersen, B.G., Finkel, R.C., Schwartz, R., Doughty, A.M., Kaplan, M.R., Schlüchter, C., 2010. Glacier advance in southern middle-latitudes during the Antarctic Cold Reversal. Nat. Geosci. 3, 700–704.
Ramos, V.A., Niemeyer, H., Skarmeta, J., Muñoz, J., 1982. Magmatic evolution of the Austral Patagonian Andes. Earth Sci. Rev. 18, 411–443.
Rasmussen, S.O., Bigler, M., Blockley, S.P., Blunier, T., Buchardt, S.L., Clausen, H.B., Cvijanovic, I., Dahl-Jensen, D., Johnsen, S.J., Fischer, H., Gkinis, V., Guillevic, M., Hoek, W.Z., Lowe, J.J., Pedro, J.B., Popp, T., Seierstad, I.K., Steffensen, J.P., Svensson, A.M., Vallelonga, P., Vinther, B.M., Walker, M.J.C., Wheatley, J.J., Winstrup, M., 2014. A stratigraphic framework for abrupt climatic changes during the Last Glacial period based on three synchronized Greenland ice-core records: refining and extending the INTIMATE event stratigraphy. Quat. Sci. Rev. 106, 14–28.
Rea, B.R., 2009. Defining modern day Area-Altitude Balance Ratios (AABRs) and their use in glacier-climate reconstructions. Quat. Sci. Rev. 28, 237–248.
Reimer, P.J., Bard, E., Bayliss, A., Beck, J.W., Blackwell, P.G., Ramsey, C.B., Buck, C.E., Cheng, H., Edwards, R.L., Friedrich, M., 2013. IntCal13 and Marine13 radiocarbon age calibration curves 0–50,000 years cal BP. Radiocarbon 55, 1869–1887.
Rovey, C.W.I., Borucki, M.K., 1995. Subglacial to proglacial sediment transition in a shallow ice-contact lake. Boreas 24, 117–127.
Sagredo, E.A., Kaplan, M.R., Araya, P.S., Lowell, T.V., Aravena, J.C., Moreno, P.I., Kelly, M.A., Schaefer, J.M., 2018. Trans-Pacific glacial response to the Antarctic Cold Reversal in the southern mid-latitudes. Quat. Sci. Rev. 188, 160–166.
Sagredo, E.A., Lowell, T.V., Kelly, M.A., Rupper, S., Aravena, J.C., Ward, D.J., Malone, A.G., 2016. Equilibrium Line Altitudes along the Andes during the Last Millennium: Paleoclimatic implications. Holocene 27, 1019–1033.
Schaller, M., von Blanckenburg, F., Veldkamp, A., Tebbens, L.A., Hovius, N., Kubik, P.W., 2002. A 30 000 yr record of erosion rates from cosmogenic ^{10}Be in Middle European river terraces. Earth Planet Sci. Lett. 204, 307–320.
Singer, C., Shulmeister, J., McLea, B., 1998. Evidence against a significant Younger Dryas cooling event in New Zealand. Science 281, 812–814.
Slaymaker, O., 2011. Criteria to Distinguish between Periglacial, Proglacial and Paraglacial Environments. Quaestiones Geographicae, p. 85.
Small, D., Fabel, D., 2015. A Lateglacial ^{10}Be production rate from glacial lake shorelines in Scotland. J. Quat. Sci. 30, 509–513.
Smedley, R., Glasser, N., Duller, G., 2016. Luminescence dating of glacial advances at Lago Buenos Aires (~ 46° S), Patagonia. Quat. Sci. Rev. 134, 59–73.
Smith, M.J., Clark, C.D., 2005. Methods for the visualisation of digital elevation models for landform mapping. Earth Surf. Process. Landforms 30, 885–900.
Smith, M.J., Paron, P., Griffiths, J.S., 2011. Chapter eight - digital mapping: visualisation, interpretation and quantification of landforms. Dev. Earth Surf. Process. 225–251. Elsevier.
Stone, J.O., 2000. Air pressure and cosmogenic isotope production. J. Geophys. Res. 105, 23753–23759.
Strelin, J., Denton, G., Vandergoes, M., Ninnemann, U., Putnam, A., 2011. Radiocarbon chronology of the Late-Glacial Puerto Bandera moraines, Southern Patagonian Icefield, Argentina. Quat. Sci. Rev. 30, 2551–2569.
Stuiver, M., Reimer, P.J., Reimer, R.W., 2009. CALIB 5.0.1. Program and documentation. http://www.calib.qub.ac.uk/.
Sugden, D.E., Bentley, M.J., Fogwill, C.J., Hulton, N.R.J., McCulloch, R.D., Purves, R.S., 2005. Late-Glacial glacier events in southernmost South America: a blend of 'Northern' and 'Southern' hemispheric climate signals? Geogr. Ann. Phys. Geogr. 87, 273–288.
Sugiyama, S., Minowa, M., Sakakibara, D., Skvarca, P., Sawagaki, T., Ohashi, Y., Naito, N., Chikita, K., 2016. Thermal structure of proglacial lakes in Patagonia. J. Geophys. Res. Earth Surf. 121, 2270–2286.
Thorndycraft, V.R., Bendle, J.M., Benito, G., Davies, B.J., Sancho, C., Palmer, A., Fabel, D., Armitage, S., Medealdea, A., Martin, J.M., 2018. Glacial lake evolution and Atlantic-Pacific drainage reversals during deglaciation of the Patagonian Ice Sheet. Quat. Sci. Rev. (in review).
Turner, K., Fogwill, C., McCulloch, R., Sugden, D.E., 2005. Deglaciation of the eastern flank of the North Patagonian Icefield and associated continental-scale lake diversions. Geogr. Ann. Phys. Geogr. 87, 363–374.
Villa-Martínez, R., Moreno, P.I., Valenzuela, M.A., 2012. Deglacial and postglacial vegetation changes on the eastern slopes of the central Patagonian Andes (47°S). Quat. Sci. Rev. 32, 86–99.
Wais Divide Project Members, 2015. Precise interpolar phasing of abrupt climate change during the last ice age. Nature 520, 661–665.
Wenzens, G., 2002. The influence of tectonically derived relief and climate on the extent of the last Glaciation east of the Patagonian ice fields (Argentina, Chile). Tectonophysics 345, 329–344.
Wenzens, G., 2003. Comment on:'The last glacial maximum and deglaciation in southern south America': by NRJ Hulton, RS Purves, RD McCulloch, DE Sugden, MJ Bentley [Quaternary science reviews 21 (2002) 233–241]. Quat. Sci. Rev. 22, 751–754.
Winsemann, J., Hornung, J.J., Meinsen, J., Asprion, U., Polom, U., Brandes, C., BUßMANN, M., Weber, C., 2009. Anatomy of a subaqueous ice-contact fan and delta complex, Middle Pleistocene, North-west Germany. Sedimentology 56, 1041–1076.
Xu, S., Dougans, A.B., Freeman, S.P., Schnabel, C., Wilcken, K.M., 2010. Improved ^{10}Be and ^{26}Al-AMS with a 5 MV spectrometer. Nucl. Instrum. Methods Phys. Res. Sect. B Beam Interact. Mater. Atoms 268, 736–738.